

1 **Rewiring the fusion oncoprotein EWS/FLI1 in Ewing sarcoma with bivalent small molecules**

2

3 Michael J. Bond<sup>\*1,2</sup>, Ryan P. Golden<sup>\*3</sup>, Giulia DiGiovanni<sup>1,2</sup>, Briana Howard<sup>1</sup>, Roman C. Sarott<sup>4</sup>,  
4 Basel A. Karim<sup>3</sup>, Sai Gourisankar<sup>4</sup>, Gabriela Alexe<sup>1,2</sup>, Kenneth Ross<sup>1,2</sup>, Nathanael S. Gray<sup>†4</sup>,  
5 Kimberly Stegmaier<sup>†1,2</sup>

6 1. Department of Pediatric Oncology, Dana-Farber Cancer Institute and Boston Children's Hospital, Boston,  
7 MA, USA

8 2. The Broad Institute of MIT and Harvard, Cambridge, MA, USA

9 3. Department of Chemistry, Stanford University, Stanford, CA, USA

10 4. Department of Chemical and Systems Biology, Stanford Cancer Institute, ChEM-H, Stanford University,  
11 Stanford, CA, USA

12 \*These authors contributed equally to this work

13 <sup>†</sup>Corresponding authors: nsgray01@stanford.edu, kimberly\_stegmaier@dfci.harvard.edu

14

15 **Abstract**

16 Deregulated transcription is a defining hallmark of cancer, especially pediatric malignancies, which  
17 are frequently driven by fusion transcription factors. Targeting transcription factors directly has been  
18 challenging as they lack druggable pockets. Recently, chemically induced proximity has enabled  
19 the rewiring of transcriptional activators to drive expression of pro-apoptotic genes using bivalent  
20 small molecules. Targeting fusion transcription factors, such as EWS/FLI1 in Ewing sarcoma, with  
21 these compounds, may open new therapeutic avenues. Here, we develop a small molecule, **EB-**  
22 **TCIP**, that recruits FKBP12<sup>F36V</sup>-tagged EWS/FLI1 to DNA sites bound by the transcriptional  
23 regulator BCL6, leading to rapid expression of BCL6 target genes. **EB-TCIP** activity is dependent  
24 on ternary complex formation and specific to cells that express FKBP-EWS/FLI1. This proof-of-  
25 concept study demonstrates that EWS/FLI1 can be relocalized on chromatin to induce genes that  
26 are ordinarily regulated by a transcriptional repressor. Insights herein will guide the development of  
27 bivalent molecules that rewire fusion transcription factors.

28

29

30

31

32 **Introduction**

33 Over the past two decades, chemical biologists have reshaped how scientists interrogate biological  
34 systems by developing tool molecules that hijack numerous enzyme classes<sup>1-7</sup>. Most recently,  
35 transcriptional activators have been rewired to drive expression of pro-apoptotic genes using  
36 **Transcriptional/epigenetic Chemical Inducers of Proximity (TCIPs)**<sup>8</sup>. Binders of known  
37 transcriptional activators BRD4 and CDK9 were linked to a B cell lymphoma 6 (BCL6) inhibitor to  
38 induce expression of pro-death genes leading to apoptosis in a lineage-specific fashion<sup>8,9</sup>. These  
39 studies have established TCIPs as a promising new therapeutic modality for cancers whose survival  
40 is dependent on suppression of apoptosis<sup>10</sup>. Hijacking fusion transcription factors (TFs) expressed  
41 only in tumor cells presents another exciting application of this technology that could be leveraged  
42 toward tumor specific therapeutic benefit.

43

44 Many cancers, but particularly pediatric malignancies, are driven by fusion TFs that are expressed  
45 solely in tumor cells and these cancers have otherwise relatively quiet genomes with few additional  
46 genetic abnormalities<sup>11-13</sup>. Therefore, directly targeting the fusion TF could yield potent therapeutic  
47 activity with a favorable toxicity profile. Ewing sarcoma (ES) is a solid tumor of the bone that is  
48 driven by a single chromosomal translocation, which results in the expression of a fusion TF  
49 comprised of the N-terminal transactivation domain of a FUS, EWS, TAF15 (FET) family RNA  
50 binding protein fused to the DNA binding domain of an E26 Transformation Specific (ETS) family  
51 TF<sup>14</sup>. ETS TFs contain a N-terminal regulatory domain and control expression of genes important  
52 for cell growth and survival<sup>15</sup>. In the FET/ETS fusion proteins that arise in ES, the fusion TF retains  
53 the ability to bind to canonical ETS target genes but acquires the strong transactivation domain of  
54 the FET protein. Moreover, the fusion TF gains the ability to bind long GGAA microsatellite repeats,  
55 where it acts as a pioneering TF, opening chromatin and establishing *de novo* enhancers that  
56 interact with promoters and boost gene expression<sup>16,17</sup>. The most common FET/ETS fusion results

57 from the (11;22)(q24;q12) translocation, which fuses the Ewing sarcoma breakpoint region 1  
58 (EWSR1) protein to the Friend leukemia integration 1 (FLI1) TF, forming the EWS/FLI1 fusion TF<sup>14</sup>.  
59  
60 EWS/FLI1 accounts for 85% of all ES cases<sup>14</sup>. As a specific and strong dependency in Ewing  
61 sarcoma based on CRISPR, RNAi, and degradation-based approaches, EWS/FLI1 should be a  
62 prime candidate for drug discovery<sup>13,14</sup>. Unfortunately, the disordered nature of the fusion TF has  
63 made it difficult to identify small molecule binders. Due to the dearth of EWS/FLI1-specific ligands,  
64 we have used a N-FKBP12<sup>F36V</sup>-EWS/FLI1 (FKBP-E/F) model system to test whether EWS/FLI1 can  
65 be relocalized to new sites on chromatin. The FKBP12<sup>F36V</sup> domain of the FKBP-E/F fusion protein  
66 binds specifically and with high affinity to *ortho*-AP1867 (**OAP**)<sup>18</sup>, which can be used as a small  
67 molecule handle to hijack FKBP-E/F activity. Given that TCIPs have successfully targeted BCL6 as  
68 a transcriptional repressor of interest (i.e., known chemical matter, validated exit vector, and assay  
69 availability) and that ES cells express this protein at moderate to high levels (Figure SI-1A), we  
70 synthesized and tested a library of bivalent molecules composed of **OAP** linked to **BI3812**, an  
71 inhibitor of BCL6. Although BCL6 is well studied in the maturation of B cells and the tumorigenesis  
72 of B cell lymphomas, its role in ES biology is less well understood. We first used genomic  
73 approaches to identify relevant BCL6 target genes in ES cells. We then used biochemical and omics  
74 approaches to characterize the ability of our lead molecule, termed **EB-TCIP**, to induce expression  
75 of ES relevant BCL6 targets and compared its activity to the effect of small molecule inhibition and/or  
76 degradation of BCL6. Our study demonstrates that EWS/FLI1 can be moved on chromatin to induce  
77 expression of neo-target genes, representing the first steps in understanding how the transcriptional  
78 machinery of EWS/FLI1 can be reprogrammed for therapeutic effect. Lessons learned from this  
79 study may inform future therapeutics for the treatment of TF-fusion driven cancers.  
80  
81  
82

83 **Results**

84 **Identifying BCL6 Target Genes in ES cells**

85 BCL6 is well-known for its oncogenic role in diffuse large B-cell lymphoma (DLBCL), where it acts  
86 as a repressor of *TP53* and associated DNA damage/proapoptotic genes, as well as cell cycle  
87 checkpoint genes such as *CDKN1A*<sup>19</sup>. Little is known about the role of BCL6 in ES tumorigenesis,  
88 and while BCL6 corepressor (BCOR) fusions are common in Ewing-like sarcomas, not much is  
89 known about the role BCL6 plays in these tumors either<sup>20</sup>. Nonetheless, DepMap expression data  
90 shows that ES cells express BCL6 at higher levels than in many other cancer types, DLBCL being  
91 an exception (Figure SI-1A) <sup>21</sup>. BCL6 is not a dependency in ES, while it is in DLBCL (Figure SI-  
92 1B).

93

94 To identify BCL6 target genes in ES cells, we used two *BCL6* targeting guides from the Avana  
95 CRISPR guide library<sup>22</sup> to knockout (KO) *BCL6* in two distinct ES models. Many cultured ES cell  
96 lines are *TP53* mutant, even though most patient tumors are *TP53* wild type<sup>13</sup>. Since BCL6  
97 represses *TP53* and related transcripts, we used RNA-seq to profile transcriptional changes in  
98 EWS502 (*TP53* mutant) and TC32 (*TP53* wild type) cells. KO of *BCL6* led to few, but consistent  
99 changes in RNA transcripts in both models (Figure 1A-B). To verify that the observed signature was  
100 related to BCL6, we performed Gene Set Enrichment Analysis (GSEA)<sup>23</sup> against a gene set derived  
101 from *BCL6* promoter binding data generated in primary B cells and DLBCL<sup>24</sup>. We observed a  
102 significant, positive correlation between both ES *BCL6* KO models and the published BCL6  
103 repressed gene set (Figure 1C-D). The two transcripts that were the most significantly upregulated  
104 in both cell lines were *SOCS2* and *CISH*. These transcripts encode for E3 ligase subunit paralogs  
105 involved in the degradation of growth hormone receptor and other cytokine receptors within the  
106 JAK/STAT signaling pathway<sup>25,26</sup>. We verified that *SOCS2* and *CISH* transcripts increase with *BCL6*  
107 KO by RT-qPCR (Figure 1E-H). Further, *SOCS2* protein levels were enhanced upon *BCL6* KO

108 (Figure 1I-J). With SOCS2 and CISH identified as *bona-fide* BCL6 repressed targets, we set out to  
109 determine if a TCIP molecule could hijack FKBP-E/F and enhance their expression.

110

111 **EB-TCIP induces BCL6 target gene expression more effectively than chemical inhibition or**  
112 **degradation of BCL6**

113 Although EWS/FLI1 has been a priority target for ES drug discovery, there has been limited success  
114 identifying EWS/FLI1 ligands. EWS/FLI1, like many TFs, is highly disordered and difficult to drug.  
115 To overcome this issue, we took advantage of N-terminal tagged FKBP12<sup>F36V</sup>-EWS/FLI1 (FKBP-  
116 E/F) cell lines that were previously developed to study EWS/FLI1 degradation using the dTAG  
117 system<sup>27,28</sup>. We envisioned that **BAK-04-212**, a bivalent molecule comprised of **OAP** and **BI3812**,  
118 which we call **EB-TCIP**, could redirect FKBP-E/F to BCL6 loci, thereby driving expression of BCL6  
119 repressed transcripts such as SOCS2 and CISH (Figure 2A-B).

120

121 We first wanted to demonstrate that **EB-TCIP** can induce a ternary complex between FKBP-E/F and  
122 BCL6 in a cell free system using time-resolved fluorescence energy transfer (TR-FRET) between  
123 the BTB domain of BCL6 (BCL6<sup>BTB</sup>) labelled with fluorescein isothiocyanate (FITC) and a His-  
124 tagged FKBP<sup>F36V</sup>, which was recognized by an anti-His-tag terbium-conjugated antibody<sup>29</sup>. **EB-TCIP**  
125 dose dependently increased TR-FRET signal with an EC<sub>50</sub> of 0.14 ± 0.03 μM, while the negative  
126 control bifunctional compound **RPG-02-089**, referred to as **NEG-1**, did not increase TR-FRET signal  
127 (Figure SI-2A). The addition of two vicinal methyl groups in **NEG-1** sterically occludes binding to the  
128 BCL6<sup>BTB</sup>. At concentrations of **EB-TCIP** above 0.31 μM a hook effect was observed. This is a  
129 characteristic property of bivalent molecules where at high concentrations, binary complexes  
130 between the compound and one target predominate over the ternary complex<sup>30</sup>. Next, we  
131 investigated formation of a ternary complex between FKBP-E/F and native BCL6. To this end, we  
132 treated EWS502 FKBP-E/F cell lysates with increasing concentrations of **EB-TCIP**. Since the FKBP-  
133 E/F construct contains a HA tag, we then used magnetic HA beads to immunoprecipitate FKBP-E/F

134 and associated proteins. We observed a dose dependent increase in the amount of BCL6 pulled  
135 down in the presence of **EB-TCIP** (Figure 2C-D). Further, **NEG-1** was unable to pulldown BCL6. By  
136 pre-treating lysates with either excess **BI3812** or **OAP** before **EB-TCIP** treatment, the ternary  
137 complex was disrupted and little BCL6 was pulled down compared to treatment with 1 or 10  $\mu$ M **EB-**  
138 **TCIP** alone (Figure 2C-D). These data demonstrate that **EB-TCIP** can form a reversible ternary  
139 complex between FKBP<sup>F36V</sup> and BCL6<sup>BTB</sup> *in vitro* and in cell lysates.

140

141 After confirmation of ternary complex formation, we next tested if **EB-TCIP** could enhance  
142 expression of BCL6 repressed targets. Previous TCIP studies monitored compound activity using a  
143 BCL6 repressed GFP reporter (Figure SI-2B)<sup>8,9</sup>. Using this same vector, we engineered an EWS502  
144 FKBP-E/F line expressing the reporter and found that **EB-TCIP** dose dependently increased the  
145 percentage of GFP positive cells to a greater extent than negative control compounds (Figure SI-  
146 2C). Next, we treated EWS502 FKBP-E/F cells with increasing concentrations of **EB-TCIP** and  
147 monitored expression of identified BCL6 targets by RT-qPCR and immunoblotting. **EB-TCIP** dose  
148 dependently increased expression of SOCS2 and CISH, with an EC<sub>50</sub> of 0.17  $\pm$  0.05  $\mu$ M and 0.11  $\pm$   
149 0.04  $\mu$ M respectively (Figure 2E-F). Maximal induction of both transcripts was reached at a  
150 concentration of 2.5  $\mu$ M with a hook effect evident at 10  $\mu$ M. **EB-TCIP** induced higher levels of  
151 expression of both transcripts compared to **BI3812** at 1  $\mu$ M. Additionally, 1  $\mu$ M of **NEG-1** did not  
152 increase SOCS2 or CISH expression. A dose dependent increase in SOCS2 protein level was also  
153 observed (Figure 2G). **EB-TCIP** induced higher SOCS2 protein expression than **BI3812** and **NEG-**  
154 1. Similar trends in transcript and protein expression were observed for TC32 FKBP-E/F cells (Fig  
155 S-2D-F, Table S1) demonstrating the activity of **EB-TCIP** is not unique to EWS502 FKBP-E/F cells.  
156 **EB-TCIP** dose dependently decreased proliferation of EWS502 FKBP-E/F cells over 72 hours  
157 (Figure SI-2G). However, we also observed similar antiproliferative activity in parental EWS502 cells  
158 that do not express exogenous FKBP-E/F (Figure SI-2H). Our viability data suggests **EB-TCIP**

159 induces off-mechanism cytotoxicity. Nonetheless, at shorter timepoints **EB-TCIP** is a useful tool  
160 molecule to study relocalization of FKBP-E/F on chromatin.

161

162 We observed a dose dependent decrease in BCL6 protein levels in both EWS502 and TC32 FKBP-  
163 E/F cells at concentrations where SOCS2 levels increase and ternary complex between FKBP-E/F  
164 and BCL6 is formed. The decrease in BCL6 protein was not due to a decrease in BCL6 transcript  
165 levels as treatment with **EB-TCIP** increased BCL6 mRNA (Figure SI-2I), which is consistent with  
166 previous TCIP studies<sup>8</sup>. We wondered if BCL6 induced degradation was enough to increase SOCS2  
167 and CISHL protein/transcript levels to the same extent as **EB-TCIP**. Therefore, we treated cells with  
168 **BI3802**<sup>31</sup> (Figure 2B), which induces the polymerization and subsequent proteasome dependent  
169 degradation of BCL6<sup>32</sup>. **BI3802** induced BCL6 degradation to a similar extent as **EB-TCIP**; however,  
170 **EB-TCIP** induced significantly higher levels of SOCS2 and *CISH* transcripts, as well as SOCS2  
171 protein, compared to **BI3802** (Figure 2H-J).

172

173 During our characterization of **EB-TCIP**, the synthesis of an **OAP** derivative that does not bind to  
174 FKBP12<sup>F36V</sup> was described<sup>33</sup>. Using this synthesis, we generated a second negative control  
175 compound, **RPG-02-205**, referred to as **NEG-2** (Figure 2B), that does not form a ternary complex  
176 but retains the ability to engage BCL6. **NEG-2** did not increase BCL6 target gene/protein expression  
177 to the same extent as **EB-TCIP** (Figure 2H-J). The activity that was observed can be attributed to  
178 **NEG-2**'s retained ability to inhibit BCL6. **NEG-2** also did not induce BCL6 degradation, providing  
179 evidence that **EB-TCIP** decreases BCL6 protein levels in a FKBP-E/F dependent manner.

180

181 Our observations above led us to hypothesize that **EB-TCIP** induces proteasome dependent  
182 degradation of BCL6. We tested this hypothesis by pre-treating EWS502 FKBP-E/F cells for 1 h  
183 with the proteasome inhibitor MG132<sup>34</sup> or the neddylation inhibitor MLN4924<sup>35</sup> before treatment with  
184 **BI3802** or **EB-TCIP** for 4 h. MG132 rescued BCL6 levels to a greater extent than MLN4924, which

185 was seen previously for **BI3802**<sup>32</sup> (Figure SI-3A). As a control we also pre-treated cells with the  
186 transcriptional inhibitor Actinomycin D<sup>36</sup> (ActD). ActD treatment abrogated **EB-TCIP** activity as  
187 expected (Figure SI-3A-C). These data suggest **EB-TCIP** activity is dependent on both active  
188 transcriptional and degradation machinery. We propose a mechanism by which a protein associated  
189 with FKBP-E/F induces BCL6 degradation, allowing FKBP-E/F to bind chromatin and drive  
190 transcription of BCL6 targets (Figure SI-3D).

191

192 **EB-TCIP induces rapid, ternary complex dependent induction of BCL6 targets that is specific**  
193 **to cells expressing FKBP-E/F**

194 To determine the kinetics of BCL6 degradation and target induction we treated EWS502 FKBP-E/F  
195 cells with DMSO, **BI3812**, **EB-TCIP**, or **BI3802** (1  $\mu$ M) over a 24 h time course. **EB-TCIP** and **BI3802**  
196 induced rapid degradation of BCL6 with near maximal degradation observed within 1 h (Figure 3A).  
197 Despite similar degradation kinetics, **EB-TCIP** enhanced SOCS2 protein levels to a greater extent  
198 than **BI3802** at all time points beyond 2 h. **EB-TCIP** also enhanced SOCS2 protein levels more than  
199 **BI3812** at these time points. Protein expression lagged behind transcript expression, which at 1 h  
200 was significantly higher in **EB-TCIP** treated cells compared to DMSO or the other molecules (Figure  
201 3B-C). **EB-TCIP**-induced expression of SOCS2 and *CISH* showed a peak between 2 and 4 h.  
202 SOCS2 expression levelled off before increasing at 24 h, whereas *CISH* expression continued to  
203 decrease until the end of the experiment. Increases in these transcripts in **BI3812** and **BI3802**  
204 treated cells were relatively stable after 2 h, suggesting **EB-TCIP** has a different mechanism of  
205 transcript induction than these compounds. These data show that **EB-TCIP** rapidly and more  
206 effectively induces expression of BCL6 targets compared to chemical inhibition or degradation.

207

208 Next, we wanted to ensure the activity of **EB-TCIP** was via a ternary complex mechanism. To do  
209 this, we pre-treated EWS502 FKBP-E/F cells with a 25-fold excess of **OAP** for 1 h before treating  
210 cells with **EB-TCIP** for 4 h. The excess **OAP** competed away **EB-TCIP** and abolished its ability to

211 induce BCL6 target expression (Figure 3D-F). Further, co-treatment with 1  $\mu$ M of **BI3812** and **OAP**  
212 did not increase BCL6 target expression as much as **EB-TCIP** (Figure 3D-F). These data show that  
213 **BI3812** and **OAP** must be chemically linked to induce a ternary complex and drive BCL6 target gene  
214 expression. To further validate the importance of ternary complex formation and show compound  
215 specificity, we tested the ability of **EB-TCIP** to increase BCL6 targets in parental, FKBP-GFP, and  
216 FKBP-E/F expressing EWS502 lines. **BI3812** induced SOCS2 protein expression in all cell lines as  
217 expected; however, **EB-TCIP** induced SOCS2 protein expression only in FKBP-E/F expressing cells  
218 (Figure 3G). Further, BCL6 target transcript levels were highest in FKBP-E/F expressing cells  
219 treated with **EB-TCIP** (Figure 3H-I). As a measure of **EB-TCIP** activity we compared the ratio of  
220 induction of transcript expression in samples treated with **EB-TCIP** or **BI3812** for each cell line. We  
221 observed a positive ratio, indicative of higher activity of **EB-TCIP** than **BI3812**, only in FKBP-E/F  
222 expressing cells. Together, these data show the enhanced ability of **EB-TCIP** to induce BCL6 target  
223 expression is dependent on ternary complex formation and FKBP-E/F expression.

224

## 225 **EB-TCIP induces rapid, dynamic changes in global transcription**

226 To profile how ternary complex formation between FKBP-E/F and BCL6 affected transcription in an  
227 unbiased manner, we treated EWS502 FKBP-E/F cells with DMSO, **BI3812**, **EB-TCIP**, or **NEG-1**  
228 (2.5  $\mu$ M) for 8 or 24 h and studied transcriptomic changes by RNA-seq. Given EWS/FLI1's ability to  
229 activate transcription, at 8 h we observed many more upregulated genes (71) than downregulated  
230 genes (4) (Figure 4A). Highly upregulated genes that we observed after *BCL6* KO, such as *SOCS2*,  
231 *CISH*, and *CXCL11*, were significantly upregulated at 8 h. The number of both upregulated (244)  
232 and down regulated genes (116) increased at 24 h with many increasing in magnitude (Figure 4B).  
233 However, some genes that were significantly upregulated at 8 h, such as *CISH*, had decreased  
234 expression at 24 h, consistent with our earlier time course data.

235

236 Global transcriptomic changes were more robust with **EB-TCIP** in comparison to DMSO, **BI3812**,  
237 and **NEG-1** (Figure 4C-D and Figure SI-4A-F). **EB-TCIP** induced the expression of more genes than  
238 both **BI3812** and **NEG-1** at 8 h. The known BCL6 targets *SOCS2* and *CXCL11* were more  
239 upregulated by **EB-TCIP** than **BI3812** or **NEG-1** at 8 h. *CISH* was significantly upregulated by **EB-**  
240 **TCIP** compared to **NEG-1**, but not **BI3812** at 8 h although expression did trend upwards (Figure  
241 4C-E). Conducting RNA-seq at an earlier timepoint may capture the kinetic difference in *CISH*  
242 expression between **EB-TCIP** and **BI3812** that we observed in our previous time course. To further  
243 asses BCL6 programming induced by **EB-TCIP** we performed GSEA comparing up-regulated genes  
244 induced by **EB-TCIP** and the transcriptional changes that result from *BCL6* KO. At both 8 and 24 h,  
245 we observed a significant positive correlation between **EB-TCIP** induced gene expression and *BCL6*  
246 KO, with *SOCS2*, *CISH*, and *CXCL11* being leading-edge genes within the enriched signature  
247 (Figure 4F). Further, at both 8 and 24 h, we observed a significant positive correlation between **EB-**  
248 **TCIP** induced gene expression and the previously published BCL6 target gene set<sup>24</sup> (Figure SI-4G-  
249 H). These data further support that **EB-TCIP** rapidly enhances BCL6 target genes compared to  
250 chemical inhibition.

251

252 **EB-TCIP relocates FKBP-E/F to BCL6 sites on chromatin**

253 To better understand the gene expression changes induced by **EB-TCIP**, we used chromatin  
254 immunoprecipitation with sequencing (ChIP-seq) to determine how **EB-TCIP** treatment changes  
255 FKBP-E/F and BCL6 localization on chromatin. EWS502 FKBP-E/F cells were treated with DMSO,  
256 **BI3812**, **BI3802** or **EB-TCIP** (1  $\mu$ M) for 24 hours and then subjected to ChIP-seq, using antibodies  
257 for HA or BCL6. A HA antibody was used instead of a FLI1 antibody to ensure only FKBP-E/F, and  
258 not endogenous EWS/FLI1, was immunoprecipitated. Globally, treatment with all compounds  
259 modestly increased FKBP-E/F on chromatin to varying degrees (Figure SI-5A). As expected,  
260 degradation of BCL6 induced by **BI3802** and **EB-TCIP** decreased BCL6 binding globally to  
261 chromatin, while inhibition with **BI3812** had minimal effect (Figure SI-5B). We observed ~50%

262 overlap between FKBP-E/F and BCL6 binding sites in DMSO treated HA and BCL6 samples (Figure  
263 SI-5C-E), and accordingly, similarities in the binding motifs of EWS/FLI1 and BCL6 (Figure SI-5G).  
264 EWS/FLI1 binds DNA at “GGAA” repeats, and this sequence is present within the recognition motif  
265 of BCL6. Further, the sequence similarity may enable FKBP-E/F to bind BCL6 target genes with  
266 greater affinity when brought into proximity by **EB-TCIP**.

267

268 To determine chromatin changes specific to **EB-TCIP** treatment, we clustered peaks in all  
269 treatments based on decreasing, unchanged, and increasing peak intensity between **EB-TCIP** and  
270 DMSO for both antibodies. This clustered analysis revealed that **EB-TCIP** induced an increase in a  
271 subset of both HA and BCL6 peaks, to a greater extent than that observed in **BI3812** or **BI3802**  
272 treated samples (Figure 5A and Figure SI-6A). We performed motif analysis to determine what DNA  
273 sequences were associated with the **EB-TCIP** treated HA increased peaks and compared this to  
274 motif analysis from global HA binding peaks in DMSO treated samples. In DMSO treated samples,  
275 the top two motifs were EWS/FLI1 related, as expected (Figure 5B) and no BCL6 motif was  
276 observed. However, the BCL6 motif was enriched in HA increased peaks and ranked 29<sup>th</sup> (Figure  
277 5C). Since **EB-TCIP** induces a ternary complex between FKBP-E/F and BCL6, we explored if the  
278 BCL6 increased peaks enriched for EWS/FLI1 signatures. BCL6 increased peaks showed  
279 enrichment in EWS/FLI1 motifs and a decrease in the rank of the BCL6 motif compared to DMSO  
280 peaks (Figure SI-6B-C).

281

282 To understand how changes in DNA binding may impact transcription globally, we compared log<sub>2</sub>fold  
283 expression of genes from our 8 h RNA-seq experiment where FKBP-E/F or BCL6 binding changed  
284 in the ChIP-seq experiments. Genes from HA increased peaks displayed increased gene expression  
285 more so at genes where both FKBP-E/F and BCL6 were bound compared to genes where only  
286 FKBP-E/F was bound. Gene expression was similar at HA decreased and HA unchanged peaks  
287 regardless of whether BCL6 was bound (Figure SI-6D). Genes from BCL6 increased peaks did not

288 show a decrease in expression, suggesting that FKBP-E/F transcriptional activation was stronger  
289 than BCL6 gene repression (Figure SI-6E).

290

291 We next visualized changes in FKBP-E/F and BCL6 binding at both BCL6 and EWS/FLI1 target  
292 gene sites. Robust BCL6 peaks were observed at *SOCS2*, *CISH*, and *CXCL11* loci in all treatments  
293 (Figure 5D-E and Figure SI-7A). FKBP-E/F binding was not observed in DMSO treated cells and  
294 only **EB-TCIP** was able to induce binding. Degradation alone does not explain increased FKBP-E/F  
295 binding as **BI3802** and **EB-TCIP** induce similar levels of BCL6 loss at *CISH*, but FKBP-E/F binding  
296 is only induced by **EB-TCIP**. Moreover, **EB-TCIP** induced FKBP-E/F binding was specific to BCL6  
297 target loci as no FKBP-E/F was observed at the *GAPDH* genomic locus (Figure-S7-B). For  
298 visualization of changes at EWS/FLI1 target sites we focused on *NR0B1* and *VRK1*, where  
299 EWS/FLI1 canonically binds at a proximal and distal enhancer respectively (Figure SI-8A-B). We  
300 observed strong FKBP-E/F binding at both enhancer sites with all treatments. However, only **EB-**  
301 **TCIP** treated samples showed increases in BCL6 binding, which mirrored the distinct pattern of  
302 FKBP-E/F at each site. Together, our ChIP-seq data shows that **EB-TCIP**, but not **BI3812** or **BI3802**,  
303 can relocalize both FKBP-E/F and BCL6 on chromatin.

304

305 Recently, small molecules have been used to redirect the pioneering TF activity of FOXA1 on  
306 chromatin<sup>37</sup>. Since **EB-TCIP** relocalizes FKBP-E/F, which has pioneering TF activity, we used assay  
307 for transposase-accessible chromatin with sequencing (ATAC-seq) to determine if chromatin  
308 accessibility is changed at genomic loci where FKBP-E/F is gained. Globally, chromatin accessibility  
309 is not significantly changed with **EB-TCIP** treatment (Figure SI-8C). However, at BCL6 target sites  
310 where FKBP-E/F is gained, such as *SOCS2*, *CISH*, and *CXCL11*, open chromatin is increased  
311 leading to increased RNA-seq peaks (Figure 5D-E and SI-7A). We also investigated changes in  
312 chromatin accessibility at BCL6 gained sites *NR0B1* and *VRK1*. EWS/FLI1 binding is relatively  
313 unaffected at these sites, as is chromatin accessibility and gene expression (Figure SI-8-A-B). Our

314 ATAC-seq data suggests that relocalized FKBP-E/F increases gene expression by opening  
315 chromatin while relocalization of BCL6 is generally not sufficient to repress EWS/FLI1 target genes.

316

317 **Discussion**

318 Although ES is the second most common bone cancer in children and adolescents, therapeutic  
319 development has been stagnant for decades. In our proof-of-concept study, we demonstrate that  
320 the pioneering TF activity of EWS/FLI1 can be redirected to genes typically inactivated by the  
321 repressor BCL6. Our tool compound **EB-TCIP**, which links **OAP** to **BI3812**, relocalized FKBP-E/F  
322 to chromatin sites bound by BCL6, thereby driving expression of genes ordinarily repressed by  
323 BCL6. The compound is potent and induces rapid transcript and protein expression of SOCS2 and  
324 *CISH*. ChIP-seq and ATAC-seq showed that **EB-TCIP** increases open chromatin at FKBP-E/F  
325 gained sites. We foresee **EB-TCIP** as being a useful tool compound to further probe the biology of  
326 ES cells in the context of relocalizing FKBP-EWS/FLI1. For example, future studies could  
327 investigate how **EB-TCIP** impacts transcriptional condensate formation, which is an important  
328 mechanism for gene activation by EWS/FLI1 and other TFs<sup>38,39</sup>. Potentially, **EB-TCIP** may be  
329 forming new transcriptional condensates that contain both EWS/FLI1 and BCL6. Although the utility  
330 of **EB-TCIP** may be limited for phenotypic measurements, as we observed off-mechanism  
331 cytotoxicity, we have also gained insights that may help inform the next generation of EWS/FLI1  
332 TCIPs, such as their proteasome dependent activity.

333

334 Our study is important because it demonstrates that TCIP molecules can bring together two DNA  
335 binding proteins. An unforeseen activity of **EB-TCIP** was its ability to induce the degradation of  
336 BCL6. We show that proteasome inhibition negates the degradation of BCL6 and impairs the activity  
337 of **EB-TCIP**. With global protein degradation inhibited, BCL6 and FKBP-E/F levels increase, which  
338 we hypothesized would increase EB-TCIP induced ternary complex and BCL6 target expression.  
339 However, we observed the opposite and since proteasome inhibition should not limit transcription,

340 these data suggest that BCL6 degradation is important for maximal activity of **EB-TCIP**. This is also  
341 corroborated by our ChIP-seq data, as we generally observed decreases in BCL6 binding at sites  
342 where FKBP-E/F binding is gained and chromatin is opened. However, BCL6 degradation alone  
343 with **BI3802** treatment is not enough to activate transcription to the same level as **EB-TCIP**. The  
344 degradation of BCL6 induced by **EB-TCIP** was competed away with excess **OAP** and not observed  
345 when cells were treated with **NEG-2**, which retains the ability to bind BCL6, suggesting that FKBP-  
346 E/F or a protein associated with FKBP-E/F, is inducing BCL6 degradation. Therefore, future  
347 EWS/FLI1 relocating TCIP molecules may also induce degradation of the targeted repressor.

348

349 Although our study focused on hijacking EWS/FLI1 TF activity, another interesting avenue of  
350 investigation would be recruiting genetic repressors to EWS/FLI1 to decrease oncogenic gene  
351 expression. Our chromatin data shows BCL6 moves to FKBP-E/F loci in a **EB-TCIP** dependent  
352 manner. Even though BCL6 is redirected to FKBP-E/F sites, some sites show increases in gene  
353 expression rather than a decrease. The inability of BCL6 to consistently repress EWS/FLI1 activated  
354 genes could be for several reasons. First, FKBP-E/F binding does not change at these sites and  
355 the transcriptional activation activity of FKBP-E/F may out compete the repressor activity of BCL6.  
356 Second, the magnitude of BCL6 gained at FKBP-E/F sites is lower (>10 fold) than the BCL6 present  
357 at SOCS2 or *CISH*. Therefore, there may not be enough BCL6 gained at these sites to repress gene  
358 expression. Finally, **EB-TCIP** uses an inhibitor of BCL6, and the BCL6 that is recruited to EWS/FLI1  
359 may not be functional (e.g., the co-repressor complex is disrupted). TCIPs containing repressor  
360 ligands that do not inhibit their function may result in bivalent molecules that can repress expression  
361 of EWS/FLI1 activated genes. Alternatively, repressors with stronger repressive function may need  
362 to be recruited.

363

364 Next generation EWS/FLI1 TCIP molecules will need to address the limitations of **EB-TCIP**. First,  
365 endogenous EWS/FLI1 will need to be recruited. Although there is a lack of ligands for EWS/FLI1,

366 future TCIPs could incorporate **MS0621**<sup>40</sup>, a recently described molecule that is reported to interact  
367 with EWSR1, EWS/FLI1, and SWI/SNF complex members. Although other molecules, such as **YK-**  
368 **4-279** and its clinical derivative **TK-216**<sup>41</sup>, are reported EWS/FLI1 inhibitors, these molecules may  
369 not be ideal ligands for TCIP development as they are also reported to destabilize microtubules at  
370 therapeutically relevant concentrations<sup>42</sup>. In light of these shortcomings, our study should  
371 encourage EWS/FLI1 ligand discovery as even functionally agnostic compounds could be used to  
372 relocalize EWS/FLI1.

373

374 Future TCIPs will need to direct EWS/FLI1 to repressors that are ES dependencies. TCIPs targeting  
375 BCL6 are antiproliferative in DLBCL because B cell lymphoma cells depend on BCL6 to evade  
376 apoptosis. BCL11B, another C2H2 zinc finger repressor, would be a good candidate for next  
377 generation EWS/FLI1 TCIPs since it is a known ES dependency<sup>43</sup>. Although there is no reported  
378 BCL11B ligand, there is precedence for targeting these proteins with regulatory domain inhibitors  
379 (i.e., **BI3812** for BCL6) or iMIDs that bind the C2H2 zinc finger in a cereblon-dependent manner<sup>44</sup>.  
380 An interesting repressor candidate in which chemical tools may already exist is ZEB2. Like BCL11B,  
381 ZEB2 is a known ES dependency<sup>45</sup>. Recently, it was shown that ZEB2 forms a complex with the  
382 lysine demethylase KDM1A in T-ALL cells<sup>46</sup>, which are also dependent on ZEB2. Presumably,  
383 KDM1A interacts with ZEB2 at genomic loci where ZEB2 acts as a repressor. There are several  
384 classes of known KDM1A inhibitors<sup>47,48</sup>, some with reported anti-proliferative activity in ES<sup>49</sup>, that  
385 could be used to recruit EWS/FLI1 to these genomic loci to enhance expression of ZEB2 repressed  
386 genes that may be more relevant to ES tumor survival.

387

388 The TCIP platform is a promising therapeutic modality for ES and other fusion TF driven cancers.  
389 Solid and hematological pediatric malignancies are driven by fusion TFs, such as PAX3/FOXO1<sup>50</sup>  
390 in rhabdomyosarcoma and CBFA2T3/GLIS2<sup>51</sup> in an aggressive subtype of acute myeloid leukemia  
391 (AML). FKBP tagged fusion TF systems could help determine if TCIPs can be used to relocalize

392 fusion TFs beyond EWS/FLI1. ES, rhabdomyosarcoma, and CBFA2T2/GLIS2 AML express fusions  
393 that are unique to the tumor cell and are not expressed in healthy cells. Therefore, TCIPs hijacking  
394 the fusion TF may have an improved therapeutic window compared to standard  
395 chemotherapies/targeted therapies as TCIPs may exhibit reduced toxicity in non-cancerous cells.  
396 Building on our proof-of-concept study, future EWS/FLI1 relocalizing TCIPs could serve as novel  
397 targeted ES therapies with improved efficacy and safety profiles for patients.

398

399 **Acknowledgements**

400 We would like to thank the Molecular Biology Core Facilities Genomics team at DFCI for sequencing  
401 our ChIP and ATAC-seq experiments. This work utilized an Illumina NovaSeq X Plus that was  
402 purchased with funding from a National Institutes of Health SIG grant 1S10OD036228. NMR spectra  
403 were acquired on NMR instruments purchased with funding from the National Institutes of Health  
404 High-End Instrumentation Grant S10OD028697-01 (Stanford ChEM-H). Additionally, this work was  
405 funded by support from National Cancer Institute R35 CA283977 and R01 CA283395 (K.S.), Cancer  
406 Moonshot U54 CA231637 (K.S. and N.S.G.), National Cancer Institute F32 CA284750 (M.J.B), and  
407 National Institute of General Medical Sciences of the National Institutes of Health T32GM136631  
408 (R.P.G). Biorender was used to make images presented in Figure 2A, SI-2B, and SI-3D.

409

410 **Disclosures**

411 K.S. previously received grant funding from the DFCI/Novartis Drug Discovery Program and is a  
412 member of the scientific advisory board (SAB) and has stock options with Auron Therapeutics on  
413 unrelated topics. Nathanael Gray is a founder, SAB member and equity holder in Syros, C4, Allorion,  
414 Lighthorse, Inception, Matchpoint, Shenandoah (board member), Larkspur (board member) and  
415 Soltego (board member). The Gray lab receives or has received research funding from Novartis,  
416 Takeda, Astellas, Taiho, Jansen, Kinogen, Arbella, Deerfield, Springworks, Interline and Sanofi.

417

418 **Materials and Methods**

419 Data Availability

420 All genome-scale dependency and expression data are available at the DepMap portal  
421 website: <https://depmap.org>. Graph Pad Prism 10 was used to calculate differences between *BCL6*  
422 expression in DLBCL vs ES (unpaired T-test with Welch's correction) and differences in *BCL6*  
423 dependency between all other cancers vs DLBCL and all other cancers vs ES (one-way ANOVA).  
424 All functional transcriptomics and genomics have been made publically available at the Gene  
425 Expression Omnibus (GEO) repository (<https://www.ncbi.nlm.nih.gov/geo/>) as GSE290895 (RNA-  
426 seq), GSE290894 (ChIP-seq), and GSE290893 (ATAC-seq).

427

428 Cell Lines and Reagents

429 All cell lines used were subject to short tandem repeat (STR) analysis for genotyping and tested for  
430 *Mycoplasma* using the MycoAlert® test kit (Lonza, LT07-318). HEK293TF cells used to generate  
431 lentivirus were purchased from Thermo Fisher Scientific (#R70007) and grown in Dulbecco's  
432 modified Eagle's medium (DMEM; Thermo Fisher Scientific, MT10013CM) supplemented with 10%  
433 fetal bovine serum (FBS; Sigma Aldrich, F2442) and 1% penicillin-streptomycin (Life Technologies,  
434 15140163). The EWS502 cell line (originally derived in Dr. J. Fletcher's Lab at Harvard University)  
435 was generously provided by Dr. Stephen L. Lessnick of Nationwide Children's Hospital and all  
436 EWS502 lines were grown in Roswell Park Memorial Institute (RPMI)-1640 medium (Life  
437 Technologies, 11875119) supplemented with 15% FBS and 1% penicillin-streptomycin. The TC32  
438 cell line (originally derived by Dr. T. Triche at UCLA School of Medicine) was generously provided  
439 by Dr. Todd Golub of the Broad Institute and Dana-Farber Cancer Institute (DFCI), and all TC32  
440 lines were grown in RPMI-1640 medium supplemented with 10% FBS and 1% penicillin-  
441 streptomycin. To passage cells for maintenance and experiments, cells were washed with sterile  
442 phosphate buffered saline (PBS; Life Technologies, 10010023) and detached with 0.05% trypsin-  
443 EDTA (Life Technologies, 25300062). Puromycin (Life Technologies, A1113803) and Blasticidin S

444   HCl (Life Technologies, A1113903) were used to select cells as indicated below. Compounds used  
445   in this work were acquired from the following sources: **BI3812** (S8735) and **MLN4924** (S7109) were  
446   purchased from Selleck Chem. **BI3802** (HY-108705) and **ortho-AP1867** (HY-114434) were  
447   purchased from Med Chem Express. **MG132** (474790) and **Actinomycin D** (A4262) were  
448   purchased from Sigma-Aldrich.

449

450   Lentiviral CRISPR/Cas9 plasmid construction

451   Parent plasmids used for guide cloning include lentiCRISPR v2-Blast (Addgene #83480) and  
452   lentiCRISPR v2-Puro (Addgene #98290). FastDigest Esp3I (BsmbI; Thermo Scientific, FD0454)  
453   was used to digest each backbone, which was then purified by gel extraction (Qiagen, 28704).  
454   Synthetic oligonucleotides encoding gene-targeting single guide RNA (sgRNA) sequences  
455   (provided below) were purchased from Integrated DNA Technologies (IDT). sgRNAs were annealed  
456   and end-phosphorylated using T4 polynucleotide kinase (New England Biolabs, M0201S) in T4 DNA  
457   Ligase Reaction Buffer containing 10 mM ATP (New England Biolabs, B0202S). Ligated vectors  
458   were transformed into One Shot Stbl3 *Escherichia coli* (Life Technologies, C737303), shaken at  
459   37 °C for 1 h, spread onto 100 µg/mL ampicillin Luria broth (LB) plates (Teknova, L1004) with a L-  
460   shaped cell spreader (Fisher Scientific, 14665230) and then grown overnight at 37 °C. Selected  
461   colonies were grown overnight in 5 mL of LB (Invitrogen, 12795-027) supplemented with 100 µg/mL  
462   ampicillin (Sigma-Aldrich, A9393). Plasmids were DNA-extracted (Qiagen, 27104) and submitted  
463   for Sanger sequencing validation at Genewiz (Azenta Life Sciences). Validated clones were cultured  
464   overnight in 250 mL volumes, and plasmids were extracted (Zymogen, D4203).

465

466   All guides used in this work were from the Broad Institute's Avana CRISPR-Cas9 library  
467   (<https://depmap.org>). The following guides sequences were used: sgFLI-2 (5'-  
468   GATCGTTGTGCCCTCCAA-3'), sgBCL6-1 (5'-AGATCCTGAGATCAACCCTG-3'), and sgBCL6-  
469   2 (5'-GATCCTGAGATCAACCCTGA-3'). As previously described<sup>52</sup>, sgChr2.2 (5'-

470 GGTGTGCGTATGAAGCAGTG-3') served as a cutting control and targets a gene desert on  
471 chromosome 2. sgLacZ (5'-AACGGCGGATTGACCGTAAT-3') served as a non-targeting,  
472 transduction control and targets a non-human gene. For ligation into the lentiCRISPRv2 (either Blast  
473 or Puro) plasmid, the additional bases 5'-CACCG-3' were added to the 5' end of the forward  
474 sequence. 5'-AAC-3' and 5'-C-3' were added at the 5' and 3' ends of the reverse sequence,  
475 respectively. sgFLI-2 was cloned into the lentiCRISPR v2-Blast plasmid. sgLacZ, sgChr2.2,  
476 sgBCL6-1, and sgBCL6-2 were cloned into the lentiCRISPR v2-Puro vector.

477

478 Generation of polyclonal FKBP-EWS/FLI1 and FKBP-GFP expressing cells

479 EWS502 cells expressing FKBP-EWS/FLI1 concurrent with knock out of endogenous EWS/FLI1  
480 (sgFLI-Ex9: 5'-GCCTCACGGCGTGCAGGAAG-3') as well as EWS502 cells expressing FKBP-GFP  
481 were generated as described previously<sup>28</sup>. TC32 cells expressing FKBP-EWS/FLI1 were generated  
482 in a similar manner, except cells were co-transduced with viral supernatants containing pLEX\_305-  
483 dTAG-EWS/FLI and lentiCRISPR v2-Blast-sgFLI-2. Cells were then selected and maintained in 1  
484 µg/mL puromycin and 10 µg/mL blasticidin. EWS502-FKBP-EWS/FLI1 cells were also maintained  
485 in 1 µg/mL puromycin and 10 µg/mL blasticidin. EWS502-FKBP-GFP cells were maintained in 1  
486 µg/mL puromycin.

487

488 Lentivirus Production and polyclonal CRISPR Cas9 KO of BCL6

489 CRISPR-Cas9 constructs were packed into lentiviral particles via transduction of HEK293TF cells  
490 in Falcon 6 well tissue culture treated plates (Corning, 353046). HEK293TF cells were seeded at a  
491 density of 400,000 cells/mL per well. The next day each well was co-transfected with 1250 ng of  
492 lentiCRISPR v2-Puro-sgRNA or FgH1tUTG-sgRNA construct plasmid, 250 ng of pVSVG plasmid  
493 (Addgene #8454), and 1250 ng of pPAX2 plasmid (Addgene #19319) using Lipofectamine 2000  
494 (Life Technologies, 11668027) according to the manufacturer's recommended protocol. Plasmids  
495 and Lipofectamine 2000 were diluted and mixed in Opti-MEM (Life Technologies, 1058021).

496 Mixtures of DNA and lipofectamine were added dropwise to each well followed by incubation for 8-  
497 16 h at 37 °C, after which media was aspirated and replaced with 3 mL of fresh DMEM. Forty-eight  
498 hours after the media change, virus-containing media was collected in 10 mL Luer-Lok syringes  
499 (BD, 302995) and sterile-filtered through 0.45 µm syringe filters (Corning, 431225). All infections  
500 were performed with freshly produced virus.

501

502 For *BCL6* KO experiments, 2 x 10<sup>6</sup> EWS502 or TC32 cells were seeded into 6-well plates in a  
503 volume of 1 mL of RPMI media supplemented with 8 or 4 µg/mL of polybrene (Santa Cruz  
504 Biotechnology, SC-134220), respectively. One mL of virus containing media was then added  
505 dropwise (final polybrene concentration of 4 or 2 µg/mL) and cells were spin-infected at 30 °C at  
506 2000 rpm for 2 h in a Sorvall Legend XTR centrifuge (Thermo Fisher Scientific). Cells were then  
507 incubated at 37 °C overnight. The next day, cells were lifted with trypsin from the 6-well plate and  
508 selected with 1 µg/mL of puromycin in a T75 flask (Thermo Fischer Scientific, 156753) for 72 h.  
509 Separate samples of non-infected cells subject to the same conditions were treated with puromycin  
510 to confirm cell death.

511

512 RNA sequencing (RNA-seq)

513 For all *BCL6* KO experiments three separate wells of cells were transduced and selected as  
514 described above. Approximately two million cells transduced with control or *BCL6* sgRNAs from  
515 each well were washed with PBS and then detached from the plate using trypsin. Half of the cells  
516 were aliquoted into a 1.5 mL Eppendorf tube and were set aside for protein purification to confirm  
517 KO. The other half of cells were pelleted by centrifugation at 2500xg for 3 min in a tabletop centrifuge  
518 (Eppendorf, 5425). Media was aspirated and total RNA was extracted using the RNAeasy Plus kit  
519 (Qiagen, 74134). Preparation of RNA-seq libraries from total RNA and sequencing was performed  
520 by Novogene (<https://en.novogene.com>). Sequencing was done at ~20 million reads per sample.  
521 Per Novogene correspondence, RNA integrity was assessed using a Bioanalyzer 2100 System

522 (Agilent Technologies). Libraries were then prepared by purifying messenger RNA (mRNA) from  
523 total RNA samples using poly-T oligo-attached magnetic beads. Purified mRNA was fragmented  
524 and library prep completed using Fast RNA seq Lib Prep Kit V2 (AbClonal Technology, RK20306).  
525 Library quality and concentration were assessed using real-time PCR and Qubit fluorometric  
526 quantitation (Thermo Fisher Scientific). Libraries were then pooled based on concentration and  
527 sequenced in 150-bp paired-end fashion on a Novaseq6000 instrument (Illumina).

528

529 For RNA sequencing experiments of EB-TCIP treated cells, 800,000 EWS502 FKBP-E/F cells were  
530 seeded into a 6 well plate. The next day, cells were treated in sextuplicate with DMSO, 2.5  $\mu$ M  
531 **BI3812**, or 2.5  $\mu$ M **EB-TCIP**, or 2.5  $\mu$ M **NEG-1**. One set of triplicates was collected as described  
532 above 8 h post treatment and the second set of triplicates was collected as described above 24 h  
533 post treatment. At both time points cells collected for RNA harvesting were frozen in 350  $\mu$ L of RLT  
534 plus buffer (Qiagen) at -80 °C. All samples were thawed at the same time and total RNA purified  
535 using the RNAeasy Plus kit. Total RNA was then subjected to library prep and RNA-seq by  
536 Novogene as described above.

537

538 Quantitative-Real Time PCR (qPCR)

539 Total RNA from 400,000 to 800,000 cells was extracted using the RNAeasy Plus kit. If cells were  
540 split for protein and RNA isolation, trypsin was used to detach cells from the plate as described  
541 earlier. For experiments where only RNA was harvested, cells were lysed in RLT plus buffer on the  
542 plate. Between 1 and 1.5  $\mu$ g of total RNA was reverse transcribed into cDNA using the High-Capacity  
543 cDNA Reverse Transcription Kit (Applied Biosystems, 4368814) and then diluted 1:5 with UltraPure  
544 DNase/RNase-Free Distilled Water (Invitrogen, 10977015). All qPCR reactions were performed  
545 using the TaqMan system (Thermo Fisher Scientific) with technical triplicate or quadruplicate.  
546 Probes used in this study include: *SOCS2*: Hs00919620\_m1, *CISH*: Hs00367082\_G1, *BCL6*:  
547 Hs00153368\_m1, and *GAPDH*: Hs02786624\_G1 (60x primer limiting). In each qPCR reaction, the

548 gene of interest was measured using FAM dye while the *GAPDH* control was measured using VIC  
549 dye. Samples were analyzed in 384-well plate format using 5  $\mu$ l of either TaqMan Universal Master  
550 Mix (Thermo Fisher Scientific, 4304437) or Fast Advanced Master Mix for qPCR (Thermo Fisher  
551 Scientific, 4444557), 0.5  $\mu$ l of FAM-emitting probe, 0.17  $\mu$ l of VIC-emitting *GAPDH* probe (60x  
552 stock), 2  $\mu$ l of diluted cDNA and 2.33  $\mu$ L of UltraPure water for a total of 10  $\mu$ l per reaction. From the  
553 10  $\mu$ L reaction volume, 8  $\mu$ L were pipetted into a MicroAmp Optical 384-well plate (Thermo Fisher  
554 Scientific, 4309849) using a 0.5-12.5  $\mu$ L E1-ClipTip electronic pipet (Thermo Scientific). The plate  
555 was spun briefly and then sealed with an optical adhesive cover (Thermo Fisher Scientific,  
556 4360954). The QuantStudio 6 Flex Real-Time PCR machine and the accompanying QuantStudio  
557 Real-Time PCR software v.1.7 (Thermo Fisher Scientific) was used to produce and analyze data.  
558 The delta-threshold cycle number ( $\Delta Ct$ ) was calculated as the difference in threshold cycle number  
559 ( $Ct$ ) between the gene of interest and *GAPDH*. The  $\Delta\Delta Ct$  was calculated as the difference between  
560 the  $\Delta Ct$  of a particular sample and the average  $\Delta Ct$  of the DMSO-treated or sgLacZ control samples.  
561 The fold change in gene expression (after *BCL6* KO or compound treatment) was calculated as the  
562 ratio of  $2^{-\Delta\Delta Ct}$  in sgLacZ cells vs other guides or DMSO treated cells vs cells treated with other  
563 compounds. Microsoft Excel was used to calculate  $\Delta Ct$ ,  $\Delta\Delta Ct$ , and fold change in gene expression.  
564  
565 One-way ANOVAs were used to compare changes in gene expression between control conditions  
566 (sgLacZ or DMSO). For time course experiments, one-way ANOVAs were used to compare the  
567 mean of **EB-TCIP** to all other conditions. For experiments comparing parental, FKBP-GFP, and  
568 FKBP-E/F cells, the ratio of **BI3812** induced expression compared to DMSO vs **EB-TCIP** induced  
569 expression compared to DMSO was calculated in Microsoft Excel. One-way ANOVA statistics were  
570 also used to compare differences between treatments for each cell type. All ANOVA statistics were  
571 calculated with Graph Pad Prism 10 using technical replicates.  
572  
573 Generation of EWS502 FKBP-EWS/FLI1 BCL6 GFP reporter and flow cytometry

574 The BCL6 GFP reporter plasmid used in previous TCIP publications<sup>8,9</sup> was graciously provided by  
575 the lab of Dr. Jerry Crabtree of Stanford University. Lentiviral particles containing the construct were  
576 produced as described above. EWS502-FKBP-EWS/FLI1 cells were infected with the lentiviral  
577 particles. Cells were selected for 72 h with 1 and 10 µg/mL of puromycin and blasticidin, respectively.  
578 After selection, cells were sorted on a BD Symphony S6 UV Cell Sorter at the DFCI Flow Cytometry  
579 Core, which yielded a polyclonal cell population with uniform GFP signal. From this population,  
580 single clones were selected by plating 0.5 cells/well into 96 well plates. After four weeks, single  
581 colonies were harvested and expanded. The clone that displayed the brightest GFP fluorescence  
582 by flow cytometry after 1 µM **EB-TCIP** treatment for 24 h was selected for further experiments.

583

584 Fifty-thousand reporter cells were plated per well in a Falcon 24 well-plate (Corning, 353047). The  
585 next day cells were treated with a dose response of **EB-TCIP**, **NEG-1**, **NEG-2**, or DMSO. Twenty-  
586 four hours later, cells were collected, filtered through Falcon Round-Bottom Polystyrene Test Tubes  
587 with Cell Strainer Snap Cap (Fisher Scientific, 0877123) and GFP intensity was measured by flow  
588 cytometry at 10,000 cells per sample on a BD FACSCelesta instrument. Live cells were gated using  
589 FSC-A and SSC-A. Data was analyzed using FlowJo v.10.4 software. Ratios of the number of cells  
590 with GFP intensity  $>10^3$  in bivalent compound treated cells vs DMSO treated cells were calculated  
591 in Microsoft Excel and are reported.

592

#### 593 Time Resolved Fluorescence Energy Transfer (TR-FRET)

594 Each reaction contained 25 nM His6-TEV-FLAG-FKBP12-F36V, 200 nM BCL6<sup>BTB</sup>-Avi-Biot, 20 nM  
595 Streptavidin-FITC (Thermo #SA1001), and 1:400 anti-6xHis terbium antibody (PerkinElmer  
596 #61HI2TLF) in 10 uL of buffer containing 20 mM HEPES, 150 mM NaCl, 0.1% BSA, 0.1% NP40,  
597 and 1 mM TCEP in a 384-well plate. Protein was incubated with drug digitally dispensed (Tecan  
598 D300e) for 1 h in the dark room at room temperature before excitation at 337 nm and measurement  
599 of emission at 520 nm (FITC) and 490 nm (terbium) with a PHERAstar FS plate reader (BMG

600 Labtech). The ratio of signal at 520 nm to 490 nm was calculated in Microsoft Excel and normalized  
601 to DMSO-treated conditions and plotted.

602

603 Protein Constructs and Purification for TR-FRET

604 Biotinylated BCL6<sup>BTB</sup>-AviTag protein used for TR-FRET assays included BCL6 amino acids 5-129  
605 with the following mutations: C8Q, C67R, C84N<sup>53</sup>. These enhance stability but do not affect the  
606 affinity for BI3812. Preparation of this protein has been described previously<sup>8</sup>.

607

608 The construct used for FKBP<sup>F36V</sup> was pNSG317 (His6-TEV-FLAG-FKBP12-F36V). Rosetta 2(DE3)  
609 (Sigma #71400) E. coli cells were transformed with plasmid and inoculated as a starter culture in  
610 50 mL Luria Broth supplemented with chloramphenicol and carbenicillin overnight. Saturated culture  
611 was divided into 2L 2XYT medium supplemented with appropriate antibiotics and grown to OD800  
612 = 0.8 at 37 °C. Protein expression was induced by addition of 400 µM IPTG (final concentration,  
613 Sigma #I678) and the temperature was adjusted from 37 °C to 18°C for overnight incubation. After  
614 incubation overnight, cells were harvested by centrifugation. Cell pellets were resuspended in ~2  
615 ml/L D800 buffer (20 mM HEPES, pH 7.5; 800 mM NaCl; 10 mM imidazole, pH 8.0; 10 % glycerol,  
616 2 mM beta mercaptoethanol) supplemented with protease inhibitors (1 mM PMSF, 1 mM  
617 benzamidine, ~20 ug/ml pepstatin, aprotinin, and leupeptin) and frozen at -80°C. Cell pellets were  
618 thawed briefly in warm water and lysed by sonication and addition of solid egg white lysozyme  
619 (Goldbio, L-040-10) before centrifugation at 16,233xg for 1 h at 12°C. Clarified lysate was mixed  
620 with ~0.5 ml/L of growth cobalt resin (Goldbio) for 1h before centrifugation at low speed to separate  
621 the beads, which were then washed by gravity flow with ~25 column volumes ice cold D800 buffer  
622 before a final wash with B50 (D800 with 50 mM NaCl) and elution with C50 (B50 with 400 mM  
623 imidazole, pH 8.0). Cobalt eluate was applied to a 5 ml anion exchange column (Q HP, Cytiva) and  
624 eluted with an 8-column volume gradient from B50 to D800. After concentration in a 3,000 MWCO  
625 Amicon filter (Millipore #UFC9003), the sample was applied to a 24 ml gel filtration column (S200

626 increase, Cytiva) primed with GF150 buffer (20 mM Tris-HCl, pH 8.5, 150 mM NaCl, 1 mM TCEP).  
627 S200 peak fractions were again concentrated by ultrafiltration, supplemented with 5% glycerol (v:v,  
628 final), and aliquoted and frozen at -80°C. A fresh aliquot was thawed for each assay.

629

630 Lysate Preparation and Immunoblotting

631 Cells were lysed in Radio Immunoprecipitation Assay (RIPA) lysis and extraction buffer (Thermo  
632 Scientific, 89900) supplemented with Halt protease inhibitor (Thermo Scientific, 87786) and Halt  
633 phosphatase inhibitor (Thermo Scientific, 78420). For on plate lysis, plates with attached cells were  
634 placed on ice for 3 min, media aspirated, and then cells were washed with ice-cold PBS. PBS was  
635 aspirated and RIPA buffer was added for 15 min with plates on ice. Cells were scraped into chilled  
636 1.5 mL Eppendorf tubes, vortexed for 20 sec and then placed on ice for 15 min, after which the  
637 lysate was vortexed for another 20 sec. Lysates were then clarified at 21,100xg for 20 min at 4 °C  
638 in a Sorvall Legend Micro 21R centrifuge (Thermo Scientific). For experiments in which protein and  
639 RNA were isolated, cells were harvested as described above. Suspended cells were placed on ice  
640 for 3 mins and then pelleted at 2500xg at 4 °C. Media was aspirated and the pellets were washed  
641 with 1 mL of ice cold PBS followed by another centrifugation at 2500xg at 4 °C. PBS was aspirated  
642 and pelleted cells were then resuspended in RIPA buffer, vortexed for 20 secs every 15 min over a  
643 30 min period, and then clarified as described above.

644

645 Lysates were prepared for gel electrophoresis by adding 4X NuPAGE LDS loading buffer (Life  
646 Technologies, NP0007) supplemented with 10% β-mercaptoethanol (BME, Sigma-Aldrich, M6250).  
647 Before addition of loading buffer, protein was quantified by colorimetric Pierce BCA assay (Thermo  
648 Scientific, 23227). One microliter of lysate was mixed with 100 µL of BCA:4% copper(iv) sulfate  
649 pentahydrate (50:1) in a Falcon 96 well plate (Corning, 353072). The plate was incubated at 37 °C  
650 for 30 min and then absorbance read at 562 nm on a Benchmark Plus microplate spectrophotometer  
651 (BioRad). The linear correlation from a standard curve of 0, 1, and 5 µg/µL was used to calculate

652 protein concentrations in Microsoft Excel. Thirty to 45 µg of protein was run on 4-15% 1.5 mm  
653 NuPAGE Bis-Tris mini pre-cast gels (Thermo Fisher Scientific, NP0336) using NuPAGE MOPS SDS  
654 Running Buffer (Thermo Fisher Scientific, NP0001). Protein was run at 80-90 V for ~20 min and  
655 then run at 130-145 V for an additional ~90 min. Once electrophoresis was complete, protein was  
656 transferred to a 0.2 µm nitrocellulose membrane (BioRad, A30741963) using the Trans-Blot Turbo  
657 System (BioRad) at 1.3 A and 25 V for 10 min. Membranes were then incubated in 1X Tris Buffered  
658 Saline (TBST; Boston BioProducts, IBB-181) for 3 min with agitation. Next, membranes were  
659 blocked for 15 mins at room temperature in EveryBlot Blocking Buffer (EBB; BioRad, 12010020).  
660 Membranes were then cut at 25 kDa and 50 kDa and incubated in primary antibody diluted in EBB  
661 supplemented with 0.02% sodium azide (Sigma-Aldrich, S2002) overnight (12-16 h) at 4 °C with  
662 agitation. The next morning membranes were washed three times with 5 mL of TBST for 5 mins per  
663 wash at room temperature. Membranes were then incubated in anti-rabbit IgG HRP-linked  
664 secondary antibody (Cell Signaling Technologies (CST), 7074S) diluted 1:10,000 in TBST for 1 h at  
665 room temperature. Next, membranes were washed three times with 5 mL of TBST for 5 mins each  
666 at room temperature. Protein signal was then visualized using SuperSignal West Femto Maximum  
667 Sensitivity Substrate (Thermo Scientific, 34096). Stable peroxide buffer was mixed 1:1 with the  
668 luminol/enhancer for 30 sec after which the blot was incubated in the mixture for 1 min before  
669 visualizing on a ChemiDoc MP Imaging System (BioRad, 10000062126) using 2x2 binning with  
670 rapid or optimal automated exposure. When probing for EWS/FLI1 after BCL6, blots were stripped  
671 using Restore Western Stripping Buffer (Life Technologies, 21059) for 1h at room temperature. Blots  
672 were washed three times with TBST for 5 mins each at room temperature and then reblocked for  
673 15 mins with EBB. EWS/FLI1 primary antibody diluted in EBB was then added, incubated overnight  
674 at 4 °C and imaged as described above. Image Lab Version 6.1.0 build 7 was used to export image  
675 files for figures.

676

677 The following primary antibodies were used at the following dilutions: rabbit monoclonal anti-SOCS2  
678 (Abcam, ab109245) at 1:1000, rabbit monoclonal anti-BCL6 (CST, 14895) at 1:1000, rabbit  
679 monoclonal anti-FLI1 (Abcam, ab133485) at 1:1000, rabbit monoclonal anti-HA (CST, 3724) at  
680 1:1000, and rabbit monoclonal anti-GAPDH (at 1:2000).

681

682 Ternary Complex Pulldowns

683 EWS502 FKBP-EWS/FLI1 cells growing on 15 cm<sup>2</sup> dishes (Thermo Scientific, 150350) were  
684 washed with PBS, lifted with trypsin, trypsin neutralized with RPMI media, and then pelleted at 1400  
685 RPM for 3 mins in an Eppendorf 5910 R centrifuge. Trypsin/media was aspirated, and the cells were  
686 washed with 5 mL of PBS and then counted using a Countess 3 cell counter (Invitrogen). Cells were  
687 then pelleted again at 1400 RPM for 3 mins, PBS was aspirated and the cells placed on ice for 5  
688 mins. Next, cells were resuspended in IP lysis buffer (20 mM Tris pH 7.5 (diluted from 1M Tris pH  
689 8.0, Invitrogen, AM9856), 150 mM NaCl (diluted from 5M, Invitrogen, AM9759), and 1% NP-40  
690 (diluted from 10%, Abcam, ab142227)) supplemented with Halt protease and phosphatase inhibitors  
691 at a concentration of 10 x 10<sup>6</sup> cells per 250 µL of lysis buffer. Lysate was kept on ice and vortexed  
692 for 20 sec every 15 mins for 1h. Lysate was transferred to a chilled 1.5 mL Eppendorf tubes and  
693 cleared at 21,100xg for 20 mins at 4 °C. Lysate was pooled into one chilled 15 mL Falcon tube and  
694 then split into 250 µL aliquots in separate, chilled tubes. Twenty-one microliters of lysate were saved  
695 as the input sample and mixed with 7 µL of 4X LDS buffer supplemented with 10% BME. Each tube  
696 of lysate was then treated with either 0.25 µL of DMSO or 1000x stock of the indicated compound.  
697 Lysate was incubated with compounds for 1 h at 4 °C with agitation. For competition experiments,  
698 lysates were pretreated with 1000x stocks of **BI3812** or **OAP** or 0.25 µL DMSO for 1 h before  
699 addition of **EB-TCIP**. While lysates incubated with compound, 25 µL of Pierce Anti-HA Magnetic  
700 Beads (Thermo Scientific, 88837) per pulldown was aliquoted into a 1.5 mL Eppendorf tube. One  
701 milliliter of IP lysis buffer was added and then the tube was placed into a DynaMag-2 magnetic rack  
702 (Invitrogen, 12321D) until the solution was clear. Buffer was removed and the beads were washed

703 twice more with 1 mL of IP lysis buffer. After the final wash, the beads were resuspended in 26  $\mu$ L  
704 of IP lysis buffer per pulldown and placed on ice. After the incubation with compounds, 25  $\mu$ L of  
705 washed beads was added to each tube. The beads were incubated with treated lysates overnight  
706 (16-24 h) at 4 °C. The next day, samples were quickly spun in a microcentrifuge and then beads  
707 separated using the magnetic rack. Beads were washed three times with ice-cold IP wash buffer  
708 (20 mM Tris pH 7.5, 150 mM NaCl, 0.01% NP-40), with quick spins in between each wash to remove  
709 liquid from the cap of the tube. After the third wash the beads were resuspended in 1.5X LDS Buffer  
710 supplemented with 2.5% BME and boiled for 10 mins at 95 °C. Boiled samples were spun at max  
711 speed in a tabletop centrifuge for 1 min to collect condensation and then placed on a magnetic rack.  
712 Supernatant was loaded into a 4-15% 1.5 mm NuPAGE Bis-Tris mini pre-cast gel and subject to  
713 electrophoresis and immunoblotting as described above.

714

715 Time Courses

716 Seven-hundred thousand EWS502 FKBP-EWS/FLI1 cells were plated into each well of four 6 well  
717 tissue culture plates. The next day, wells were treated in sextuplicate with either DMSO, 1  $\mu$ M  
718 **BI3812**, 1  $\mu$ M **EB-TCIP**, or 1  $\mu$ M **BI3802**. Cells were then harvested at each time point by  
719 trypsinization as described above. At each time point half the cells were collected for RNA extraction  
720 and the other half used for protein isolation. RNA samples were frozen at -80 °C in RLT plus buffer  
721 while protein samples were frozen at -80 °C in RIPA buffer. All RNA or protein samples were thawed  
722 at the same time and processed together in a single batch. Purified RNA was subject to RT-qPCR  
723 as described above. Lysates were subject to immunoblotting as described above.

724

725 Competition Assay

726 One million, two hundred thousand EWS502 FKBP-EWS/FLI1 cells were plated into each well of  
727 two 6 well tissue culture plates. The next day, cells were treated with either DMSO or 25  $\mu$ M **OAP**  
728 (free acid) for 1h at 37 °C. After this pretreatment, media was aspirated and cells were treated with

729 either DMSO, 25  $\mu$ M **OAP**, 1  $\mu$ M **BI3812**, 1  $\mu$ M **EB-TCIP**, 25  $\mu$ M **OAP** plus 1  $\mu$ M **EB-TCIP**, or 1  $\mu$ M  
730 **BI3812** plus 1  $\mu$ M **OAP** for an additional 4 h at 37 °C. Cells were then harvested by trypsinization  
731 as described above. Half the cells were collected for RNA extraction and the other half used for  
732 protein isolation. RNA samples were frozen at -80°C in RLT plus buffer while protein samples were  
733 frozen at -80 °C in RIPA buffer. All RNA or protein samples were thawed at the same time and  
734 processed together. Purified RNA was subject to RT-qPCR as described above. Lysates were  
735 subject to immunoblotting as described above.

736

737 Ubiquitin/Proteasome & Transcription Inhibitor Treatment

738 One million, two hundred thousand EWS502 FKBP-EWS/FL1 cells were plated into each well of  
739 three 6 well tissue culture plates. The next day, cells were treated with DMSO, 1  $\mu$ M **MG132**, 1  $\mu$ M  
740 **MLN4924**, or 1  $\mu$ M **Actinomycin D** for 1 h at 37 °C. After pre-treatment, media was aspirated and  
741 cells were treated with either DMSO, 1  $\mu$ M **EB-TCIP**, or 1  $\mu$ M **BI3802** plus and minus each inhibitor  
742 for an additional 4 h at 37 °C. Cells were then harvested by trypsinization. Half the cells were  
743 collected for RNA extraction and the other half used for protein isolation. RNA samples were frozen  
744 at -80 °C in RLT plus buffer while protein samples were frozen at -80 °C in RIPA buffer. All RNA or  
745 protein samples were thawed at the same time and processed together. Purified RNA was subject  
746 to RT-qPCR as described above. Lysates were subject to immunoblotting as described above.

747

748 Chromatin-Immunoprecipitation sequencing (ChIP-seq)

749 Eleven million EWS502 FKBP-EWS/FL1 cells were plated into 15 cm<sup>2</sup> dishes. The next day cells  
750 were treated with DMSO, 1  $\mu$ M **BI3812**, 1  $\mu$ M **EB-TCIP**, or 1  $\mu$ M **BI3802** in quadruplicate. After 24  
751 h, media was aspirated, and cells were harvested by trypsinization as described above. Cells from  
752 two 15 cm<sup>2</sup> plates treated with the same condition were pooled and counted. Forty million EWS502  
753 FKBP-EWS/FL1 cells per condition (20 million cells per ChIP reaction) were collected in a 50 mL  
754 Falcon tube. Cells were pelleted at 300xg for 5 mins and then washed twice in 5 ml PBS. Cells were

755 then crosslinked by resuspension in 10 mL PBS containing 1% methanol-free formaldehyde  
756 (Thermo Fisher Scientific, 28906) and rotated slowly by hand for 10 mins at room temperature. The  
757 reaction was quenched by addition of 1 mL of 2.5 M glycine (Sigma Aldrich, G7126). Cells were  
758 pelleted at 800xg for 5 mins at 4 °C pellets and then washed twice with 10 mL PBS at room  
759 temperature supplemented with 1 mM PMSF. After resuspending in the second wash, the cell  
760 suspension was split into two chilled 50 mL Falcon tubes (5 mL each). After spinning at 800xg for 5  
761 mins and removing the second PBS wash, cell pellets were flash frozen in liquid nitrogen. When  
762 processing samples one set of tubes for all conditions was thawed on ice and a pulldown for either  
763 HA or BCL6 was performed as described below.

764

765 For each immunoprecipitation (IP), 100 µl of protein A Dynabeads (Thermo Fisher Scientific,  
766 10002D) was washed three times in 1 ml BSA blocking solution (0.5% w/v sterile-filtered BSA in  
767 UltraPure H<sub>2</sub>O) and resuspended in 250 µl BAS blocking solution. Beads were pooled and then 10  
768 µg of either anti-HA (Cell Signaling Technologies, 86124SF) or anti-BCL6 antibody (Thermo Fischer  
769 Scientific, PA5-27390) per IP was added. Two micrograms of spike-in antibody recognizing a  
770 Drosophila-specific histone variant was added (Active Motif, 61686) to normalize samples. The  
771 following morning, the antibody-conjugated beads were washed four times in 1 ml BSA blocking  
772 solution and then resuspended in 100 µl of the solution per IP and stored at 4 °C.

773

774 Frozen, crosslinked cells were thawed briefly on ice and then resuspended in 1 ml of SDS lysis  
775 buffer (0.5% SDS, 5 mM EDTA, 50 mM Tris-HCl pH 8.0, 100 mM NaCl, and 0.2% sodium azide)  
776 supplemented with Halt protease inhibitor and incubated at room temperature for 2 min with gentle  
777 agitation. Lysates were transferred to microcentrifuge tubes and centrifuged at 15,000xg for 10 mins  
778 at 4 °C. The nuclear pellet was re-suspended in 950 µl of ChIP IP buffer (2 parts SDS lysis buffer  
779 and 1 part Triton dilution buffer, which was composed of 100 mM Tris-HCl pH 8.0, 100 mM NaCl,  
780 5 mM EDTA, 0.2% NaN<sub>3</sub> and 5% Triton X-100) supplemented with Halt protease inhibitor. Nine-

781 hundred microliters was then transferred to a milliTUBE (Covaris, 520130). Sonication was  
782 performed on an E220 Focus Ultra sonicator (Covaris) at 5% duty cycle, 140 W peak power, 200  
783 cycles per burst, at 4 °C for 25 mins per milliTUBE. Sheared chromatin was transferred to a 1.5 ml  
784 tube and centrifuged at 15,000xg for 10 mins at 4 °C. The supernatant of sheared chromatin was  
785 transferred to a new reaction tube. To prepare the ChIP DNA input sample, 5 µl of sheared chromatin  
786 was transferred to a PCR strip-tube (USA Scientific, 1402-4700) and mixed with 40 µl de-  
787 crosslinking buffer (100 mM NaHCO3 and 1% SDS buffer), 1 µl RNase A (Thermo Fisher Scientific,  
788 12091021) and 1 µl proteinase K (Thermo Fisher Scientific, AM2546). The tube was incubated for  
789 2 h at 65 °C in a ProFlex PCR thermal cycler (Applied Biosystems) to de-crosslink DNA–protein  
790 covalent bonds. DNA was isolated using Agencourt AMPure XP bead-based purification at a 1.2  
791 times ratio (Beckman Coulter, A63881). Briefly, beads were mixed with the sample in the PCR tube  
792 and incubated for 10 mins at room temperate. Tubes were then placed in a magnetic separation  
793 rack (EpiCypher, 10-0008) and washed twice with 500 µL of 80% ethanol. DNA was then eluted in  
794 50 µl Tris-EDTA (SigmaAldrich, 93283) and stored at –20 °C. To the remainder of sheared chromatin  
795 was added 100 µL of conjugated bead–antibody solution was. Before addition of the antibody bound  
796 beads, 40 ng per reaction of *Drosophila* spike-in chromatin (ActiveMotif, 53083) was added to the  
797 pooled antibody bound beads. IP reactions were rotated overnight at 4 °C.

798

799 The following day, ChIP reactions were washed twice in 1 ml low-salt buffer (0.1% SDS, 1% Triton  
800 X-100, 2 mM EDTA, 20 mM Tris-HCl pH 8.0, and 150 mM NaCl), high-salt buffer (0.1% SDS, 1%  
801 Triton X-100, 2 mM EDTA, 20 mM Tris-HCl pH 8.0, and 500 mM NaCl), lithium chloride buffer (0.25 M  
802 LiCl, 1% IGEPAL-CH 630, 1% sodium deoxycholate, 10 mM Tris-HCl pH 8.0, and 1 mM EDTA) and  
803 then once in 700 µl ice-cold Tris-EDTA buffer (Sigma Aldrich, 93283). Chromatin was eluted using  
804 100 µl fresh ChIP elution buffer (1% SDS and 0.1 M NaHCO3) and rotated at room temperature for  
805 15 mins. Eluate was transferred to PCR tubes and mixed with 8 µl 2.5 M NaCl, 1 µl RNase A and  
806 1 µl proteinase K. Samples were de-crosslinked for 12–16 h at 65 °C in a thermal cycler. ChIP DNA

807 was extracted from the de-crosslinked samples using AMPure XP beads at a 1.2 $\times$  ratio as described  
808 above and eluted in 20  $\mu$ l of Tris-EDTA. DNA was quantified using a Qubit dsDNA high sensitivity  
809 assay (Q32851). DNA fragment sizes were measured with a Tapestation 2200 instrument (Agilent,  
810 ScreenTape, 5067-5584; reagents, 5067-5585).

811

812 ChIP-seq libraries were prepared using a NEBNext Ultra II DNA Library Kit for Illumina sequencing  
813 (NEB, E7645S) and NEBNext Multiplex Oligos for Illumina sequencing (NEB, E6440S). HA and  
814 BCL6 samples were PCR-amplified for 12 cycles. Library pooling and indexing was evaluated with  
815 shallow sequencing on an Illumina MiSeq. Subsequently, libraries were sequenced on an Illumina  
816 NovaSeq X Plus targeting roughly 40 million, 150bp read pairs per sample by the Molecular Biology  
817 Core Facilities at Dana-Farber Cancer Institute.

818

819 Assay for Transposase-accessible chromatin with sequencing (ATAC-seq)

820 Three-hundred thousand EWS502 FKBP-EWS/FLI1 cells were plated into each well of a 12-well  
821 tissue culture plate. The next day cells were treated with DMSO or 1  $\mu$ M **EB-TCIP** in duplicate. After  
822 24 h, cells were harvested by trypsinization as described above and counted. Next, 100,000 cells  
823 from each sample were used to prepare libraries for ATAC-seq using a commercially available kit  
824 (ActiveMotif, 53150). The molarity of each library was calculated using a Qubit dsDNA Broad Range  
825 Assay kit (Thermo Fisher Scientific, Q32850) and an Agilent TapeStation 2200. Library pooling and  
826 indexing was evaluated with shallow sequencing on an Illumina MiSeq. Subsequently, libraries were  
827 sequenced on an Illumina NovaSeq X Plus targeting roughly 20 million, 150bp read pairs per sample  
828 by the Molecular Biology Core Facilities at Dana-Farber Cancer Institute.

829

830 Cell Viability

831 Fifty microliters of a 10,000 cell/mL suspension of EWS502 or EWS502 FKBP-EWS/FLI1 were  
832 seeded into each well of a white polystyrene 384 well cell culture plates (Corning, 3570). The next

833 day cells were treated with DMSO, **OAP**, **BI3812**, or **EB-TCIP** using a HP D300e Digital Dispenser.  
834 Cells were treated with 8-point dose responses starting at 10  $\mu$ M with 1:2 dilutions. Treated cells  
835 were incubated for 72 h at 37 °C, after which 10  $\mu$ L of Cell-Titer-Glo (Promega, G7573) was added  
836 to each well using a 2-125  $\mu$ L E1-ClipTip electronic pipet (Thermo Scientific). The plate was then  
837 incubated at room temperature for 15 mins with 350 rpm rotation in an Eppendorf MixMate.  
838 Luminescence was determined using a CLARIOStar Plus plate reader (BMG Labtech). The ratio of  
839 between luminescence of compound treated samples to DMSO treated samples was calculated in  
840 Microsoft Excel. Dose response curves were then generated by fitting the data to an [inhibitor] vs.  
841 dose response non-linear regression using GraphPad Prism 10.

842

843 RNA-seq data analysis

844 RNA-seq data analysis was performed according to the ENCODE standards  
845 (<https://www.encodeproject.org/data-standards/rna-seq/long-rnas/> ). Quality check of unaligned  
846 reads was performed using FastQC v.0.11.9  
847 (<https://www.bioinformatics.babraham.ac.uk/projects/fastqc/>) and MultiQC v.1.14<sup>54</sup> respectively.  
848 Using STAR v.2.7.11a<sup>55</sup> the paired end reads were aligned to hg38/gencodev30 with standard  
849 parameters –outSAMtype BAM SortedByCoordinate --outSAMunmapped None --  
850 outSAMattributes NH HI NM MD AS XS --outReadsUnmapped FastX --outSAMstrandField  
851 intronMotif --quantMode TranscriptomeSAM GeneCounts --quantTranscriptomeBan  
852 IndelSoftclipSingleend --readFilesCommand zcat. Gene level reads were counted and summarized  
853 across hg38 exons by using featureCounts v.2.0.3 from the Subread v2.0.0 package  
854 (<https://subread.sourceforge.net/>). Following alignment, quality control checks were performed  
855 using SARTools v.1.7.3<sup>56</sup>. DESeq2 v.1.44.0 was used to normalize gene counts and quantify  
856 differential expression between experimental and control conditions<sup>57</sup> using the apeglm v1.26.1<sup>57</sup>  
857 library. Gene level expression was estimated as  $\log_2(\text{TPM} + 1)$  normalized reads. Expressed genes  
858 were identified as genes with maximum  $\log_2(\text{TPM} + 1)$  expression  $\geq 1$  across conditions. Gene

859 differential expression status (decrease, increase or not significant change) was estimated based  
860 on shrunken  $\log_2$  fold change scores with the cutoffs  $|\text{fold change expression}| \geq 1.5$  and adjusted  $P$   
861  $\leq 0.10$ . Heatmaps displaying transcriptional changes were created using the Morpheus software  
862 platform (<https://software.broadinstitute.org/morpheus/>) based on  $\log_2(\text{fold change})$  expression  
863 data.

864

865 Gene set enrichment analysis

866 GSEA software v.4.2.2<sup>23</sup> was used to identify signature enrichment of experimental conditions in  
867 *BCL6* KO, compound treatment, and corresponding conditions. MSigDB v7.4 collections, a  
868 published *BCL6* target gene set<sup>24</sup>, and in-house curated gene sets were analyzed for enrichment  
869 against the data. For each experimental condition, the expressed genes were ranked based on the  
870 expression fold change in sg*BCL6* vs sg*Chr2.2* or compound treated versus DMSO control. Results  
871 were visualized with volcano plots with Normalized Enrichment Score (NES) versus  $-\log_{10}(P)$  and  
872 GSEA plots. Significance cutoffs for GSEA enrichments:  $|\text{NES}| \geq 1.3$ ,  $P \leq 0.10$ , FDR  $\leq 0.25$ .

873

874 ChIP-Seq data analysis

875 The analysis of the spiked-in ChIP-Seq data was performed according to the ENCODE standards  
876 (<https://www.encodeproject.org/chip-seq/>). Quality control was performed on unmapped sequences  
877 using FastQC v.0.11.9 (<https://www.bioinformatics.babraham.ac.uk/projects/fastqc/>) and MultiQC  
878 v.1.14<sup>54</sup>. Adapters and low-quality reads were removed using Trimmomatic v0.39<sup>58</sup>. Reads were  
879 mapped to the human genome (GRCh38/hg38) and to the spike-in *Drosophila melanogaster* (dm6)  
880 using bowtie2 v.2.5.1<sup>59</sup> with the “local very\_sensitive” parameters. Mapped reads were processed  
881 with SAMtools v0.1.19<sup>60</sup> and reads with low mapping quality (MAPQ < 5) were disregarded.  
882 Duplicate reads were removed using the Picard Mark Duplicates method implemented in the  
883 sambamba 0.7.1 tool<sup>61</sup>. Fragment size distributions were computed using the PEFragmentSize tool  
884 available in the deepTools v.3.5.1 package<sup>62</sup>.

885

886 Human and *Drosophila* genome-wide counts across 2000 bp bins were computed with the  
887 bamSummary tool available in the deepTools package v.3.5.0<sup>62</sup>. Bins with at least 10 reads in less  
888 than 3 samples and bins overlapping ENCODE blacklisted regions were excluded. The Active Motif  
889 Spike-in Normalization protocol was then applied to compute the scaling factors per antibody  
890 samples as ratios between the average dm6 counts across antibody samples vs. the dm6 counts  
891 for that sample. The normalization factor was set to 1 if the percentage of *Drosophila* reads was  
892 less than the 1% minimum cutoff.

893

894 The bamCoverage tool from the deepTools package v.3.5.0<sup>62</sup> was used to generate normalized  
895 reads per kilobase per million (RPKM) genome-wide coverage bigwig files with specified bin sizes  
896 of 20 bp and scaled with the pre-computed spike-in scale factors.

897

898 Peak calling was performed using the model-based MACS2 v.2.1.1.20160309<sup>63</sup> software against  
899 experimental inputs with a significance cutoff FDR  $\leq 0.01$ . Bwtool software<sup>64</sup> was used to compute  
900 the area under the curve (AUC) for the RPKM normalized signal across genomic regions. MACS2  
901 peaks were filtered by removing binding regions with low AUC coverage of  $[\log_2(\text{AUC}+1) < 14]$  and  
902 ENCODE hg38 black-list regions (<https://www.encodeproject.org/annotations/ENCSR636HFF/>).  
903 Various mapping and genomic analyses including indexing, sorting, intersection, and merging were  
904 executed using SAMtools v.1.9 and Bedtools v.2.29<sup>65,66</sup>. Next, quality control for peaks called was  
905 performed using ChIPQC<sup>67</sup> under the Bioconductor package v.3.9. Homer v4.11<sup>68</sup> platform was  
906 used to annotate peaks called with the closest hg38 genes using the annotatePeaks function. Peak  
907 binding signal were visualized using the Integrative Genomic Viewer (IGV) v.2.12.3<sup>69</sup>. Promoter  
908 regions were defined as the area of the genome  $\pm 3.0\text{kb}$  from gene transcription start sites (TSS).

909

910 Antibody binding sites identified by MACS2 were merged into a set of aggregated peaks for control  
911 and treatments across conditions. Utilizing deepTools multiBamSummary tool, peak by sample  
912 counts was generated. Counts were used to perform differential peak analysis. Changes between  
913 two conditions binding signal were identified as increase, decrease or not significant based on  
914 absolute cutoff of 1.5 for delta area under curve. Significance of changes for binding reads was  
915 calculated by using DESeq2 v.1.44.0 with a cutoff of  $P \leq 0.10$ .

916

917 Heatmaps of normalized AUC signal were created using deepTools v.3.5.1 computeMatrix and  
918 plotHeatmap functions. Metaplots displaying average normalized scores across genomic regions  
919 were created using deepTools v.3.5.1 plotProfile function. Motif enrichment analysis was performed  
920 using Homer v.4.11<sup>68</sup>.

921

922 Box plots of Supplemental Figure SI-6 D-G used Homer annotatePeak genes to map peaks in  
923 increasing, decreasing, and unchanged groups to genes from DESeq2 analysis shrunken log2 fold  
924 change values. HA peak groups in Supplemental Figure SI-6 D-E were subdivided using bedtools  
925 by whether they overlapped with the merged AUC filtered BCL6 peaks. BCL6 peak groups in  
926 Supplemental Figure SI-6 F-G were subdivided using bedtools by whether they overlapped with the  
927 merged AUC filtered HA peaks. Genes with peaks from the increase or decrease groups were  
928 excluded from the no change group. Using the R pairwise.t.test function, a paired t-test with a  
929 Benjamini-Hochberg correction was used to evaluate the significance for the differences of the RNA-  
930 seq LFC distributions for the various peak categories.

931

### 932 ATAC-Seq data analysis

933 ATAC-Seq analysis was performed according to the ENCODE standards  
934 (<https://www.encodeproject.org/atac-seq/>). Quality control was performed on the unmapped paired  
935 end reads with FastQC v.0.11.9 (<https://www.bioinformatics.babraham.ac.uk/projects/fastqc/>) and

936 MultiQC v.1.14<sup>54</sup>. Adapters were then trimmed and filtered using Trimmomatic v.0.36<sup>58</sup>. Using  
937 bowtie2 v.2.5.1, the trimmed paired end reads were aligned to the hg38 genome with the -local -  
938 very\_sensitive -X 2000 parameters. Reads mapped to the hg38 genome to chromosomes 1 to 22  
939 with a MAPQ > 5 were kept. Duplicates were removed using Picard Mark Duplicates method  
940 implemented in the sambamba 0.7.1 tool<sup>61</sup>. deepTools v.3.5.1<sup>62</sup> AlignemntSieve tool was used to  
941 shift reads 4bp on the positive strand and -5bp on the negative strand. Replicate correlations were  
942 calculated and visualized using multiBamsummary and bamCorrelate, along with fragment size  
943 distributions using PEFragmentSize within the deepTools v.3.5.1 package<sup>62</sup>. Replicates were  
944 merged and then peak calling was performed with MACS2 v.2.1.1.20160309<sup>63</sup>. Next, AUC binding  
945 signal was computed with the bwtool program<sup>64</sup>. The Homer v.4.11<sup>68</sup> program was employed to  
946 annotate called peaks to the closest hg38 genes using the annotatePeaks function. Promoter  
947 regions were defined as the area of the genome  $\pm 3.0\text{kb}$  from gene transcription start sites (TSS).  
948 Peak binding signal was visualized using the Integrative Genomic Viewer (IGV) v.2.12.3<sup>69</sup>.

949

950

951

952

953

954

955

956

957

958

959

960

961

962

## References:

- 963 1 Sakamoto, K. M. *et al.* Protacs: chimeric molecules that target proteins to the Skp1-Cullin-F  
964 box complex for ubiquitination and degradation. *Proc Natl Acad Sci U S A* **98**, 8554-8559,  
965 doi:10.1073/pnas.141230798 (2001).
- 966 2 Siriwardena, S. U. *et al.* Phosphorylation-Inducing Chimeric Small Molecules. *J Am Chem  
967 Soc* **142**, 14052-14057, doi:10.1021/jacs.0c05537 (2020).
- 968 3 Henning, N. J. *et al.* Deubiquitinase-targeting chimeras for targeted protein stabilization. *Nat  
969 Chem Biol* **18**, 412-421, doi:10.1038/s41589-022-00971-2 (2022).
- 970 4 Chen, P. H. *et al.* Modulation of Phosphoprotein Activity by Phosphorylation Targeting  
971 Chimeras (PhosTACs). *ACS Chem Biol* **16**, 2808-2815, doi:10.1021/acschembio.1c00693  
972 (2021).
- 973 5 Costales, M. G., Suresh, B., Vishnu, K. & Disney, M. D. Targeted Degradation of a Hypoxia-  
974 Associated Non-coding RNA Enhances the Selectivity of a Small Molecule Interacting with  
975 RNA. *Cell Chem Biol* **26**, 1180-1186 e1185, doi:10.1016/j.chembiol.2019.04.008 (2019).
- 976 6 Bond, M. J. & Crews, C. M. Proteolysis targeting chimeras (PROTACs) come of age: entering  
977 the third decade of targeted protein degradation. *RSC Chem Biol* **2**, 725-742,  
978 doi:10.1039/d1cb00011j (2021).
- 979 7 Liu, X. & Ciulli, A. Proximity-Based Modalities for Biology and Medicine. *ACS Cent Sci* **9**, 1269-  
980 1284, doi:10.1021/acscentsci.3c00395 (2023).
- 981 8 Gourisankar, S. *et al.* Rewiring cancer drivers to activate apoptosis. *Nature* **620**, 417-425,  
982 doi:10.1038/s41586-023-06348-2 (2023).
- 983 9 Sarott, R. C. *et al.* Relocalizing transcriptional kinases to activate apoptosis. *Science* **386**,  
984 eadl5361, doi:10.1126/science.adl5361 (2024).
- 985 10 Bradner, J. E., Hnisz, D. & Young, R. A. Transcriptional Addiction in Cancer. *Cell* **168**, 629-  
986 643, doi:10.1016/j.cell.2016.12.013 (2017).
- 987 11 Melendez, B. *et al.* Methods of measurement for tumor mutational burden in tumor tissue.  
988 *Transl Lung Cancer Res* **7**, 661-667, doi:10.21037/tlcr.2018.08.02 (2018).
- 989 12 Liu, Y. *et al.* Etiology of oncogenic fusions in 5,190 childhood cancers and its clinical and  
990 therapeutic implication. *Nat Commun* **14**, 1739, doi:10.1038/s41467-023-37438-4 (2023).
- 991 13 Crompton, B. D. *et al.* The genomic landscape of pediatric Ewing sarcoma. *Cancer Discov* **4**,  
992 1326-1341, doi:10.1158/2159-8290.CD-13-1037 (2014).
- 993 14 Grunewald, T. G. P. *et al.* Ewing sarcoma. *Nat Rev Dis Primers* **4**, 5, doi:10.1038/s41572-018-  
994 0003-x (2018).
- 995 15 Sizemore, G. M., Pitarresi, J. R., Balakrishnan, S. & Ostrowski, M. C. The ETS family of  
996 oncogenic transcription factors in solid tumours. *Nat Rev Cancer* **17**, 337-351,  
997 doi:10.1038/nrc.2017.20 (2017).
- 998 16 Bailly, R. A. *et al.* DNA-binding and transcriptional activation properties of the EWS-FLI-1  
999 fusion protein resulting from the t(11;22) translocation in Ewing sarcoma. *Mol Cell Biol* **14**,  
1000 3230-3241, doi:10.1128/mcb.14.5.3230-3241.1994 (1994).
- 1001 17 Johnson, K. M., Taslim, C., Saund, R. S. & Lessnick, S. L. Identification of two types of GGAA-  
1002 microsatellites and their roles in EWS/FLI binding and gene regulation in Ewing sarcoma.  
1003 *PLoS One* **12**, e0186275, doi:10.1371/journal.pone.0186275 (2017).
- 1004 18 Clackson, T. *et al.* Redesigning an FKBP-ligand interface to generate chemical dimerizers  
1005 with novel specificity. *Proc Natl Acad Sci U S A* **95**, 10437-10442,  
1006 doi:10.1073/pnas.95.18.10437 (1998).
- 1007 19 McLachlan, T. *et al.* B-cell Lymphoma 6 (BCL6): From Master Regulator of Humoral Immunity  
1008 to Oncogenic Driver in Pediatric Cancers. *Mol Cancer Res* **20**, 1711-1723, doi:10.1158/1541-  
1009 7786.MCR-22-0567 (2022).
- 1010 20 Peters, T. L. *et al.* BCOR-CCNB3 fusions are frequent in undifferentiated sarcomas of male  
1011 children. *Mod Pathol* **28**, 575-586, doi:10.1038/modpathol.2014.139 (2015).

- 1012 21 Tsherniak, A. *et al.* Defining a Cancer Dependency Map. *Cell* **170**, 564-576 e516, doi:10.1016/j.cell.2017.06.010 (2017).
- 1013 22 Sanson, K. R. *et al.* Optimized libraries for CRISPR-Cas9 genetic screens with multiple modalities. *Nat Commun* **9**, 5416, doi:10.1038/s41467-018-07901-8 (2018).
- 1014 23 Subramanian, A. *et al.* Gene set enrichment analysis: a knowledge-based approach for interpreting genome-wide expression profiles. *Proc Natl Acad Sci U S A* **102**, 15545-15550, doi:10.1073/pnas.0506580102 (2005).
- 1015 24 Ci, W. *et al.* The BCL6 transcriptional program features repression of multiple oncogenes in primary B cells and is deregulated in DLBCL. *Blood* **113**, 5536-5548, doi:10.1182/blood-2008-12-193037 (2009).
- 1016 25 Sobah, M. L., Liongue, C. & Ward, A. C. SOCS Proteins in Immunity, Inflammatory Diseases, and Immune-Related Cancer. *Front Med (Lausanne)* **8**, 727987, doi:10.3389/fmed.2021.727987 (2021).
- 1017 26 Vesterlund, M. *et al.* The SOCS2 ubiquitin ligase complex regulates growth hormone receptor levels. *PLoS One* **6**, e25358, doi:10.1371/journal.pone.0025358 (2011).
- 1018 27 Nabet, B. *et al.* The dTAG system for immediate and target-specific protein degradation. *Nat Chem Biol* **14**, 431-441, doi:10.1038/s41589-018-0021-8 (2018).
- 1019 28 Nabet, B. *et al.* Rapid and direct control of target protein levels with VHL-recruiting dTAG molecules. *Nat Commun* **11**, 4687, doi:10.1038/s41467-020-18377-w (2020).
- 1020 29 Gourisankar, S. *et al.* Author Correction: Rewiring cancer drivers to activate apoptosis. *Nature* **621**, E27, doi:10.1038/s41586-023-06543-1 (2023).
- 1021 30 Riching, K. M., Caine, E. A., Urh, M. & Daniels, D. L. The importance of cellular degradation kinetics for understanding mechanisms in targeted protein degradation. *Chem Soc Rev* **51**, 6210-6221, doi:10.1039/d2cs00339b (2022).
- 1022 31 Kerres, N. *et al.* Chemically Induced Degradation of the Oncogenic Transcription Factor BCL6. *Cell Rep* **20**, 2860-2875, doi:10.1016/j.celrep.2017.08.081 (2017).
- 1023 32 Slabicki, M. *et al.* Small-molecule-induced polymerization triggers degradation of BCL6. *Nature* **588**, 164-168, doi:10.1038/s41586-020-2925-1 (2020).
- 1024 33 Hu, Z. *et al.* EGFR targeting PhosTACs as a dual inhibitory approach reveals differential downstream signaling. *Sci Adv* **10**, eadj7251, doi:10.1126/sciadv.adj7251 (2024).
- 1025 34 Tsubuki, S. *et al.* Purification and characterization of a Z-Leu-Leu-Leu-MCA degrading protease expected to regulate neurite formation: a novel catalytic activity in proteasome. *Biochem Biophys Res Commun* **196**, 1195-1201, doi:10.1006/bbrc.1993.2378 (1993).
- 1026 35 Soucy, T. A. *et al.* An inhibitor of NEDD8-activating enzyme as a new approach to treat cancer. *Nature* **458**, 732-736, doi:10.1038/nature07884 (2009).
- 1027 36 Sobell, H. M. Actinomycin and DNA transcription. *Proc Natl Acad Sci U S A* **82**, 5328-5331, doi:10.1073/pnas.82.16.5328 (1985).
- 1028 37 Won, S. J. *et al.* Redirecting the pioneering function of FOXA1 with covalent small molecules. *Mol Cell* **84**, 4125-4141 e4110, doi:10.1016/j.molcel.2024.09.024 (2024).
- 1029 38 Zuo, L. *et al.* Loci-specific phase separation of FET fusion oncoproteins promotes gene transcription. *Nat Commun* **12**, 1491, doi:10.1038/s41467-021-21690-7 (2021).
- 1030 39 Sanalkumar, R. *et al.* Highly connected 3D chromatin networks established by an oncogenic fusion protein shape tumor cell identity. *Sci Adv* **9**, eabo3789, doi:10.1126/sciadv.abo3789 (2023).
- 1031 40 Vital, T. *et al.* MS0621, a novel small-molecule modulator of Ewing sarcoma chromatin accessibility, interacts with an RNA-associated macromolecular complex and influences RNA splicing. *Front Oncol* **13**, 1099550, doi:10.3389/fonc.2023.1099550 (2023).
- 1032 41 Spriano, F. *et al.* The ETS Inhibitors YK-4-279 and TK-216 Are Novel Antilymphoma Agents. *Clin Cancer Res* **25**, 5167-5176, doi:10.1158/1078-0432.CCR-18-2718 (2019).
- 1033 42 Povedano, J. M. *et al.* TK216 targets microtubules in Ewing sarcoma cells. *Cell Chem Biol* **29**, 1325-1332 e1324, doi:10.1016/j.chembiol.2022.06.002 (2022).

- 1063 43 Wiles, E. T., Lui-Sargent, B., Bell, R. & Lessnick, S. L. BCL11B is up-regulated by EWS/FLI  
1064 and contributes to the transformed phenotype in Ewing sarcoma. *PLoS One* **8**, e59369,  
1065 doi:10.1371/journal.pone.0059369 (2013).
- 1066 44 Sievers, Q. L. *et al.* Defining the human C2H2 zinc finger degrome targeted by thalidomide  
1067 analogs through CCRN. *Science* **362**, doi:10.1126/science.aat0572 (2018).
- 1068 45 Wiles, E. T., Bell, R., Thomas, D., Beckerle, M. & Lessnick, S. L. ZEB2 Represses the  
1069 Epithelial Phenotype and Facilitates Metastasis in Ewing Sarcoma. *Genes Cancer* **4**, 486-  
1070 500, doi:10.1177/1947601913506115 (2013).
- 1071 46 Goossens, S. *et al.* Oncogenic ZEB2 activation drives sensitivity toward KDM1A inhibition in  
1072 T-cell acute lymphoblastic leukemia. *Blood* **129**, 981-990, doi:10.1182/blood-2016-06-721191  
1073 (2017).
- 1074 47 Sacilotto, N. *et al.* Comprehensive in Vitro Characterization of the LSD1 Small Molecule  
1075 Inhibitor Class in Oncology. *ACS Pharmacol Transl Sci* **4**, 1818-1834,  
1076 doi:10.1021/acspctsci.1c00223 (2021).
- 1077 48 Noce, B., Di Bello, E., Fioravanti, R. & Mai, A. LSD1 inhibitors for cancer treatment: Focus on  
1078 multi-target agents and compounds in clinical trials. *Front Pharmacol* **14**, 1120911,  
1079 doi:10.3389/fphar.2023.1120911 (2023).
- 1080 49 Pishas, K. I. *et al.* Therapeutic Targeting of KDM1A/LSD1 in Ewing Sarcoma with SP-2509  
1081 Engages the Endoplasmic Reticulum Stress Response. *Mol Cancer Ther* **17**, 1902-1916,  
1082 doi:10.1158/1535-7163.MCT-18-0373 (2018).
- 1083 50 Skapek, S. X. *et al.* Rhabdomyosarcoma. *Nat Rev Dis Primers* **5**, 1, doi:10.1038/s41572-018-  
1084 0051-2 (2019).
- 1085 51 Gruber, T. A. *et al.* An Inv(16)(p13.3q24.3)-encoded CBFA2T3-GLIS2 fusion protein defines  
1086 an aggressive subtype of pediatric acute megakaryoblastic leukemia. *Cancer Cell* **22**, 683-  
1087 697, doi:10.1016/j.ccr.2012.10.007 (2012).
- 1088 52 Malone, C. F. *et al.* Selective Modulation of a Pan-Essential Protein as a Therapeutic Strategy  
1089 in Cancer. *Cancer Discov* **11**, 2282-2299, doi:10.1158/2159-8290.CD-20-1213 (2021).
- 1090 53 Stead, M. A. *et al.* Structure of the wild-type human BCL6 POZ domain. *Acta Crystallogr Sect  
1091 F Struct Biol Cryst Commun* **64**, 1101-1104, doi:10.1107/S1744309108036063 (2008).
- 1092 54 Ewels, P., Magnusson, M., Lundin, S. & Kaller, M. MultiQC: summarize analysis results for  
1093 multiple tools and samples in a single report. *Bioinformatics* **32**, 3047-3048,  
1094 doi:10.1093/bioinformatics/btw354 (2016).
- 1095 55 Dobin, A. *et al.* STAR: ultrafast universal RNA-seq aligner. *Bioinformatics* **29**, 15-21,  
1096 doi:10.1093/bioinformatics/bts635 (2013).
- 1097 56 Varet, H., Brillet-Gueguen, L., Coppee, J. Y. & Dillies, M. A. SARTools: A DESeq2- and EdgeR-  
1098 Based R Pipeline for Comprehensive Differential Analysis of RNA-Seq Data. *PLoS One* **11**,  
1099 e0157022, doi:10.1371/journal.pone.0157022 (2016).
- 1100 57 Love, M. I., Huber, W. & Anders, S. Moderated estimation of fold change and dispersion for  
1101 RNA-seq data with DESeq2. *Genome Biol* **15**, 550, doi:10.1186/s13059-014-0550-8 (2014).
- 1102 58 Bolger, A. M., Lohse, M. & Usadel, B. Trimmomatic: a flexible trimmer for Illumina sequence  
1103 data. *Bioinformatics* **30**, 2114-2120, doi:10.1093/bioinformatics/btu170 (2014).
- 1104 59 Langmead, B. & Salzberg, S. L. Fast gapped-read alignment with Bowtie 2. *Nat Methods* **9**,  
1105 357-359, doi:10.1038/nmeth.1923 (2012).
- 1106 60 Danecek, P. *et al.* Twelve years of SAMtools and BCFtools. *Gigascience* **10**,  
1107 doi:10.1093/gigascience/giab008 (2021).
- 1108 61 Tarasov, A., Vilella, A. J., Cuppen, E., Nijman, I. J. & Prins, P. Sambamba: fast processing of  
1109 NGS alignment formats. *Bioinformatics* **31**, 2032-2034, doi:10.1093/bioinformatics/btv098  
1110 (2015).
- 1111 62 Ramirez, F. *et al.* deepTools2: a next generation web server for deep-sequencing data  
1112 analysis. *Nucleic Acids Res* **44**, W160-165, doi:10.1093/nar/gkw257 (2016).
- 1113 63 Zhang, Y. *et al.* Model-based analysis of ChIP-Seq (MACS). *Genome Biol* **9**, R137,  
1114 doi:10.1186/gb-2008-9-9-r137 (2008).

- 1115 64 Pohl, A. & Beato, M. bwtool: a tool for bigWig files. *Bioinformatics* **30**, 1618-1619,  
1116 doi:10.1093/bioinformatics/btu056 (2014).
- 1117 65 Li, H. *et al.* The Sequence Alignment/Map format and SAMtools. *Bioinformatics* **25**, 2078-  
1118 2079, doi:10.1093/bioinformatics/btp352 (2009).
- 1119 66 Quinlan, A. R. & Hall, I. M. BEDTools: a flexible suite of utilities for comparing genomic  
1120 features. *Bioinformatics* **26**, 841-842, doi:10.1093/bioinformatics/btq033 (2010).
- 1121 67 Carroll, T. S., Liang, Z., Salama, R., Stark, R. & de Santiago, I. Impact of artifact removal on  
1122 ChIP quality metrics in ChIP-seq and ChIP-exo data. *Front Genet* **5**, 75,  
1123 doi:10.3389/fgene.2014.00075 (2014).
- 1124 68 Heinz, S. *et al.* Simple combinations of lineage-determining transcription factors prime cis-  
1125 regulatory elements required for macrophage and B cell identities. *Mol Cell* **38**, 576-589,  
1126 doi:10.1016/j.molcel.2010.05.004 (2010).
- 1127 69 Thorvaldsdottir, H., Robinson, J. T. & Mesirov, J. P. Integrative Genomics Viewer (IGV): high-  
1128 performance genomics data visualization and exploration. *Brief Bioinform* **14**, 178-192,  
1129 doi:10.1093/bib/bbs017 (2013).
- 1130

1131

1132

1133

1134

1135

1136

1137

1138

1139

1140

1141

1142

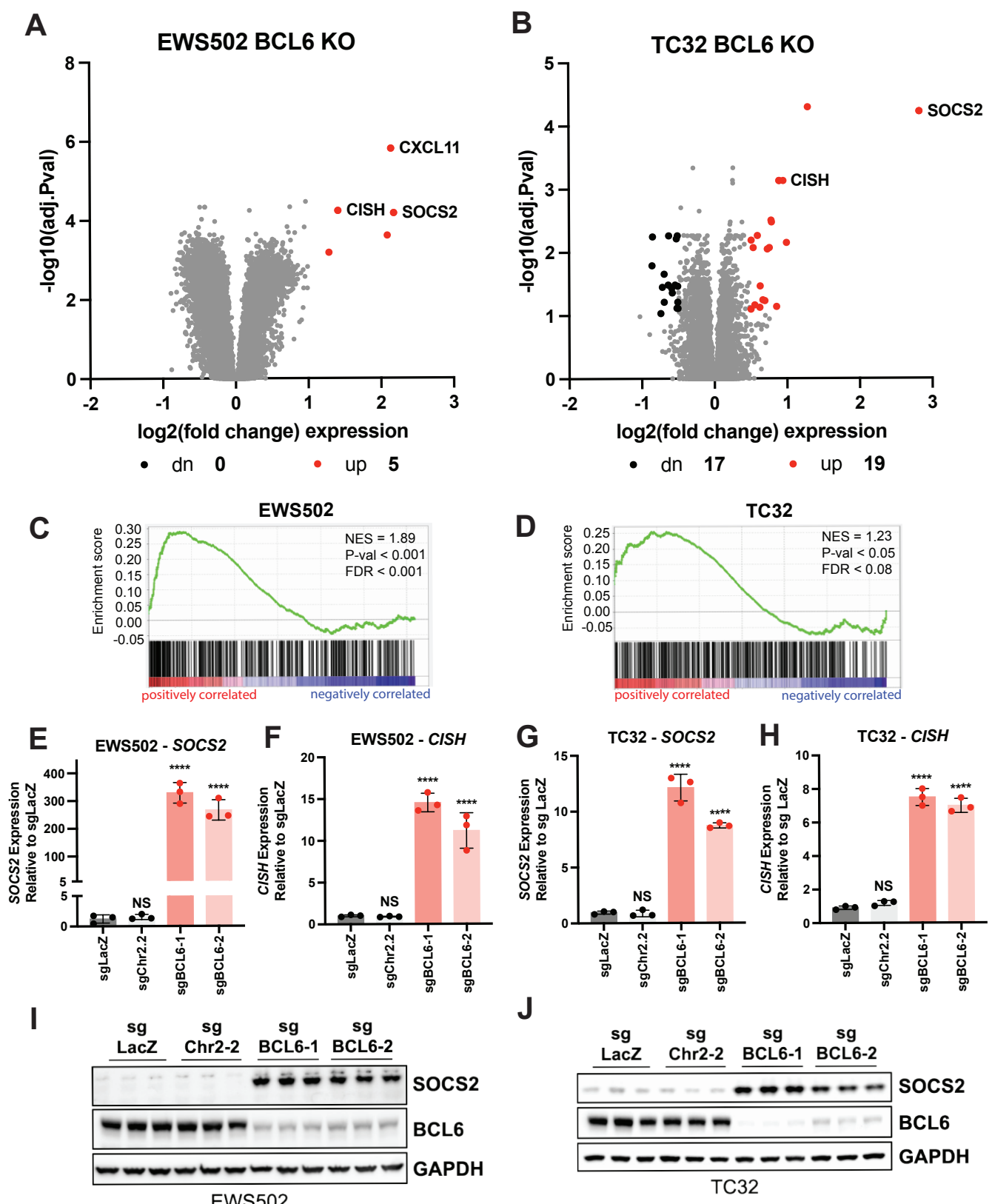
1143

1144

1145

1146

1147



1148 **Figure 1: Determining BCL6 target genes in ES.** Volcano plots of differentially expressed RNA  
 1149 species in *BCL6* KO (two guides averaged over three replicates per guide) EWS502 cells (A) or  
 1150 TC32 cells (B) vs Chr2.2 control cells. GSEA in EWS502 (C) or TC32 (D) *BCL6* KO cells shows a  
 1151 positive correlation with a published *BCL6* gene signature derived from *BCL6* promoter binding

1152 data<sup>24</sup>. SOCS2 and *CISH* transcripts have increased expression by RT-qPCR in *BCL6* KO EWS502  
1153 cells (E and F) or TC32 cells (G and H) vs control guides. Average expression from three  
1154 independent cell transductions (performed in technical triplicate) is shown. RT-qPCR data was  
1155 compared by one-way ANOVA; NS = not significant, \*\*\*\* p < 0.001. All error bars in the figure show  
1156 mean ± SD. Immunoblotting shows *BCL6* KO and corresponding increase in SOCS2 protein levels  
1157 in EWS502 (I) and TC32 (J) cells. Each lane is from an independent transduction of cells. GAPDH  
1158 serves as a loading control.

1159

1160

1161

1162

1163

1164

1165

1166

1167

1168

1169

1170

1171

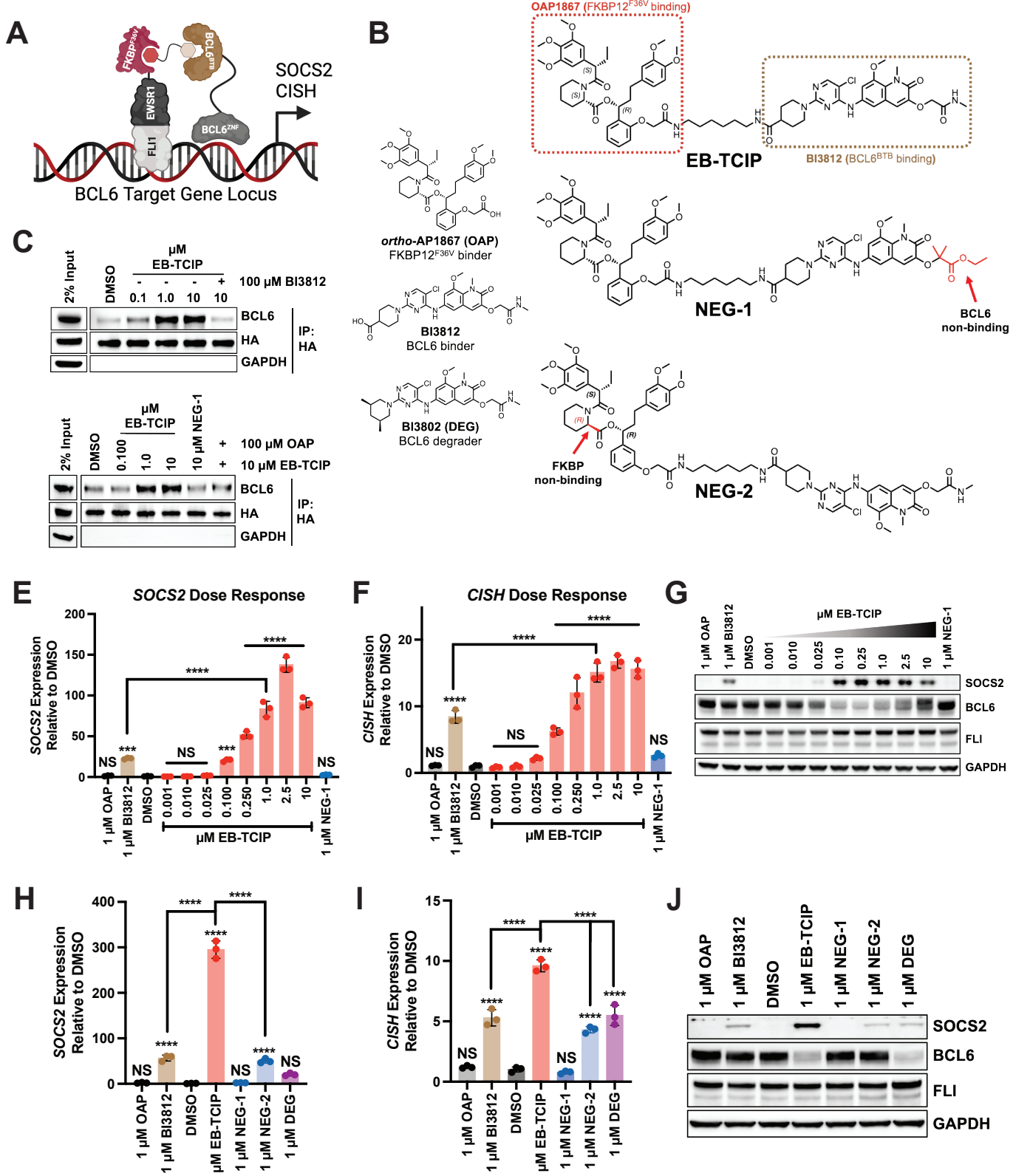
1172

1173

1174

1175

1176



1177 **Figure 2: EB-TCIP increases expression of BCL6 target genes in ES cells at nanomolar**  
1178 **concentrations.** (A) Schematic of EB-TCIP mechanism of action. EB-TCIP induces a ternary

1179 complex between FKBP12<sup>F36V</sup> tagged EWS/FL1 and BCL6, which leads to activation of BCL6 target

1180 gene transcription. Image made with Biorender. (B) Structures of compounds used in this work. (C)

1181 **EB-TCIP** increases the association of BCL6 with **EB-TCIP** in a dose dependent manner in EWS502  
1182 FKBP-E/F cell lysates while **NEG-1** (D) does not induce a ternary complex. The association is  
1183 reversible as excess **BI3812** (C) and excess **OAP** (free acid) (D) abrogate ternary complex  
1184 formation. GAPDH was probed to determine if unbound proteins were removed by washing. **EB-**  
1185 **TCIP** dose dependently increases SOCS2 (E) and *CISH* (F) expression by RT-qPCR. (G) SOCS2  
1186 protein levels dose dependently increase while BCL6 protein levels dose dependently decrease  
1187 after **EB-TCIP** treatment. **EB-TCIP** induces higher SOCS2 (H) and *CISH* (I) transcript levels than  
1188 chemical inhibition with **BI3812** or chemically induced degradation with **BI3802 (DEG)**. (J) SOCS2  
1189 protein levels are highest in **EB-TCIP** treated cells compared to **BI3812**, **BI3802 (DEG)**, or negative  
1190 control compounds that do not form ternary complexes. Immunoblotting is representative of three  
1191 biological replicates and GAPDH serves as a loading control. All experiments were performed in  
1192 FKBP-E/F expressing EWS502 cells. RT-qPCR experiments show one experiment with technical  
1193 triplicate that is representative of three biological replicates. Means of SOCS2 and *CISH* expression  
1194 were compared using one-way ANOVA with multiple comparisons; NS = not significant, \*\*\* p <  
1195 0.005, \*\*\*\* p < 0.001. All error bars in the figure indicate mean  $\pm$  SD. Unless indicated with brackets,  
1196 significance above each condition indicates comparison of that mean to the mean of DMSO.

1197

1198

1199

1200

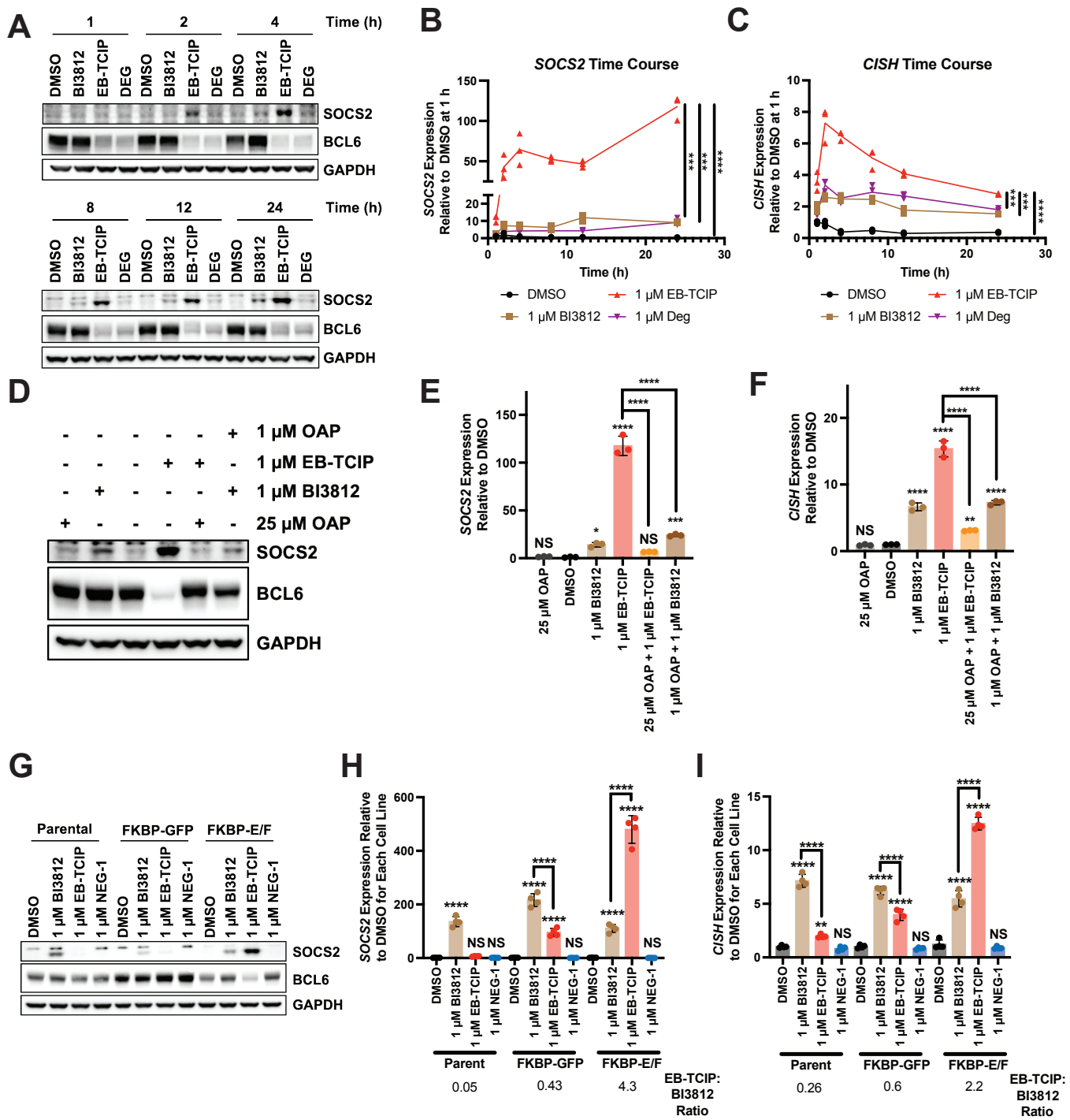
1201

1202

1203

1204

1205



1206 **Figure 3: EB-TCIP activity is rapid, ternary complex dependent, and specific to cells**  
1207 **expressing FKBP-E/F.** (A) Time course of SOCS2 and BCL6 protein levels. BCL6 degradation  
1208 occurs within 1 h for both **EB-TCIP** and **BI3802 (DEG)**. **EB-TCIP** induces SOCS2 expression by 2  
1209 h and maintains higher expression levels than **BI3812** or **BI3802 (DEG)** throughout the time course.  
1210 SOCS2 (B) and *CISH* (C) transcripts reach a maximum between 2 and 4 h by RT-qPCR. (D) **EB-**  
1211 **TCIP** induced SOCS2 protein expression can be reversed with 25-fold excess **OAP** (free acid). Co-

1212 treatment of 1  $\mu$ M **BI3812** and **OAP** do not increase SOCS2 protein expression more than 1  $\mu$ M  
1213 **BI3812** alone. **EB-TCIP** induced SOCS2 (E) and *CISH* (F) transcript expression is reversed with  
1214 excess **OAP**. **BI3812** and **OAP** must be chemically linked to induce maximum transcript expression.  
1215 (G) **EB-TCIP** induces the highest expression of SOCS2 protein in EWS502 FKBP-E/F cells  
1216 compared to EWS502 parental cells or EWS502 cells expressing FKBP-GFP. Only treatment with  
1217 **EB-TCIP** induces more expression of SOCS2 (H) and *CISH* (I) than **BI3812** in EWS502 FKBP-E/F  
1218 cells. **EB-TCIP:BI3812** ratio was calculated by dividing the average expression of each transcript in  
1219 **EB-TCIP** treated cells by the average expression of each transcript in **BI3812** treated cells.  
1220 Immunoblotting is representative of three biological replicates. RT-qPCR experiments show one  
1221 experiment with technical triplicate or quadruplicate that is representative of three biological  
1222 replicates. The means of SOCS2 and *CISH* expression were compared using one-way ANOVA with  
1223 multiple comparisons; NS = not significant, \*  $p < 0.05$ , \*\*  $p < 0.01$ , \*\*\*  $p < 0.005$ , \*\*\*\*  $p < 0.001$ . All  
1224 error bars in the figure represent mean  $\pm$  SD. Unless indicated with brackets, significance above  
1225 each condition indicates comparison of that mean to the mean of DMSO. In (H) and (I), unless  
1226 indicated with brackets, the means of **BI3812**, **EB-TCIP**, and **NEG-1** were compared to the DMSO  
1227 sample for the corresponding cell line.

1228

1229

1230

1231

1232

1233

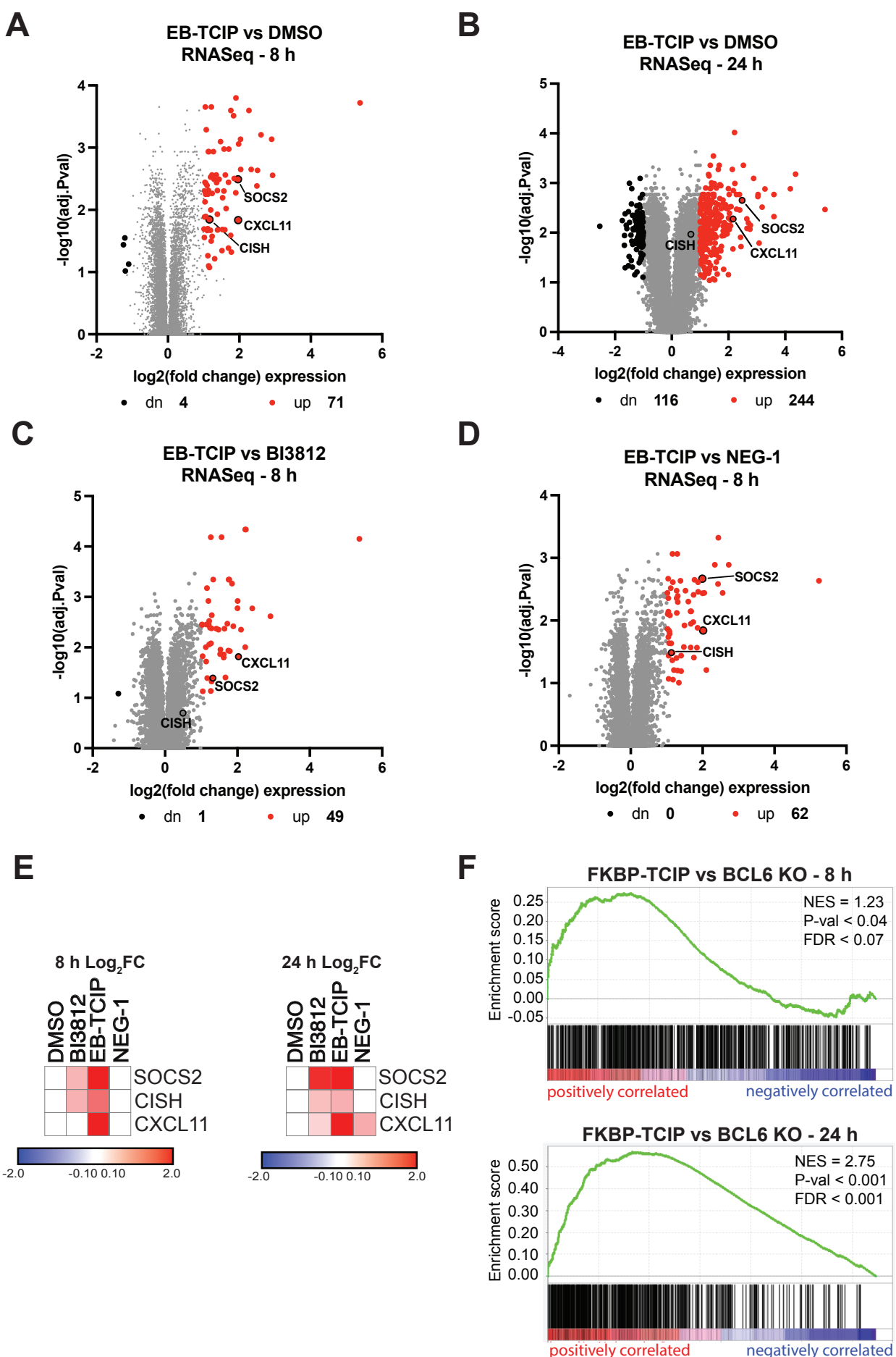
1234

1235

1236

1237

1238



1239 **Figure 4: Global RNA changes induced by EB-TCIP are similar to genetic KO of BCL6 in**  
1240 **EWS502 cells.** Volcano plots portraying log<sub>2</sub>fold changes of gene expression from cells treated with  
1241 2.5  $\mu$ M **EB-TCIP** versus DMSO at 8 (A) and 24 (B) h with a -log<sub>10</sub> adjusted P-value cut off of 1. **EB-**  
1242 **TCIP** treatment predominantly increases expression of transcripts at both timepoints. Volcano plots  
1243 portraying log<sub>2</sub> fold changes of cells treated with 2.5  $\mu$ M **EB-TCIP** versus 2.5  $\mu$ M **BI3812** (C) or 2.5  
1244  $\mu$ M **NEG-1** (D) at 8 hours with a -log<sub>10</sub> P-value cut off of 1. **EB-TCIP** induces higher expression of  
1245 BCL6 transcripts than **BI3812** or **NEG-1** at this early timepoint. Dots corresponding to SOCS2,  
1246 *CISH*, and *CXCL11* are labelled with black borders. (E) Heatmaps of changes in BCL6 target gene  
1247 expression at 8 (left) and 24 h (right) show that **EB-TCIP** induces faster and/or higher expression of  
1248 these select genes. (F) GSEA comparing EB-TCIP treated EWS502 FKBP-E/F cells to *BCL6* KO  
1249 EWS502 parental cells at 8 (top) and 24 h (bottom) show significant positive correlation between  
1250 the two gene sets. RNA-seq data is shown as the average of three independent replicates.

1251

1252

1253

1254

1255

1256

1257

1258

1259

1260

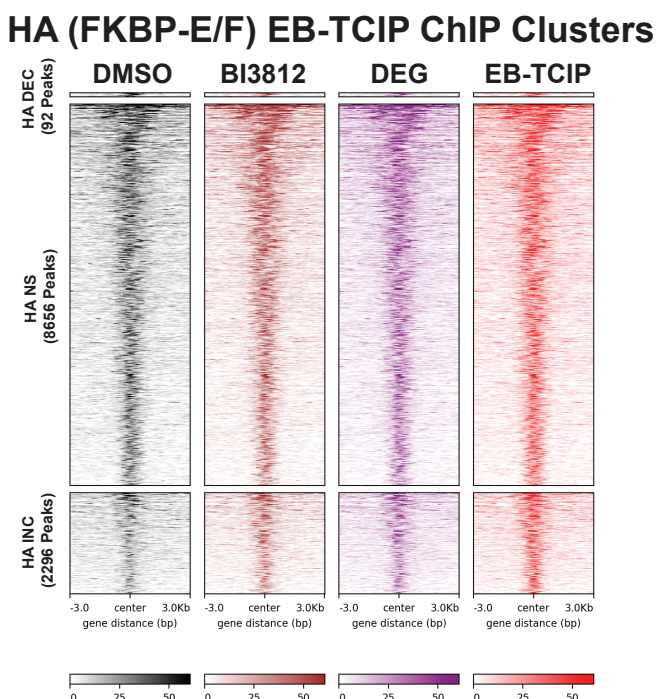
1261

1262

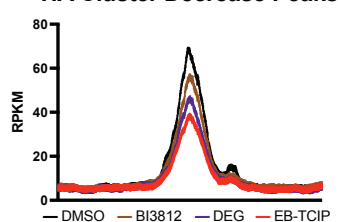
1263

1264

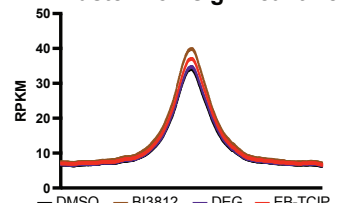
**A**



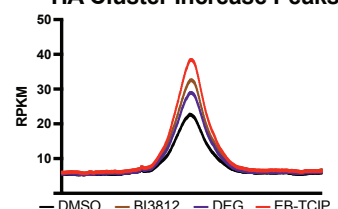
**HA Cluster Decrease Peaks**



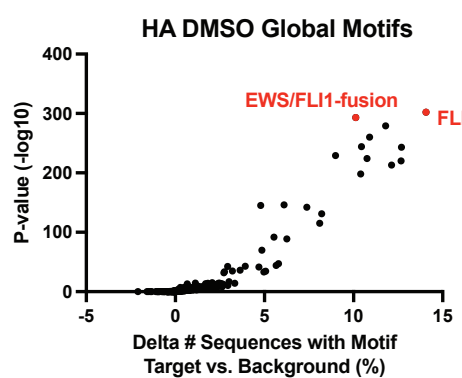
**HA Cluster Non-significant Peaks**



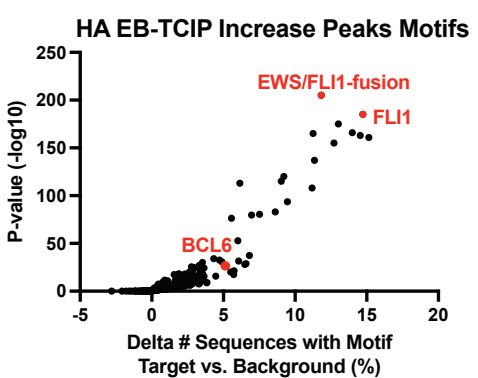
**HA Cluster Increase Peaks**



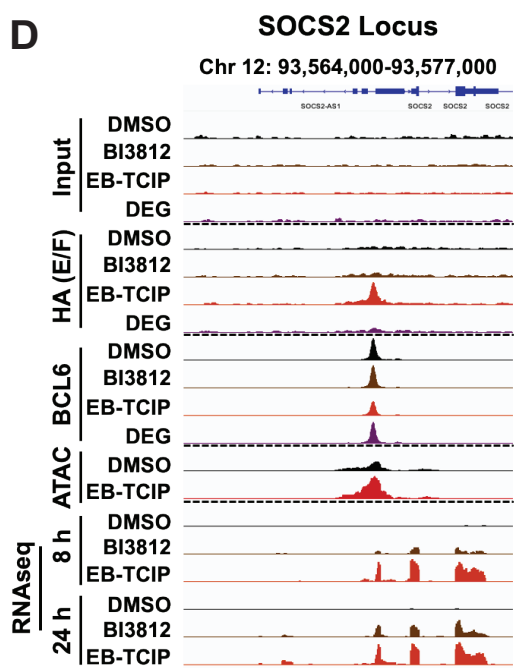
**B**



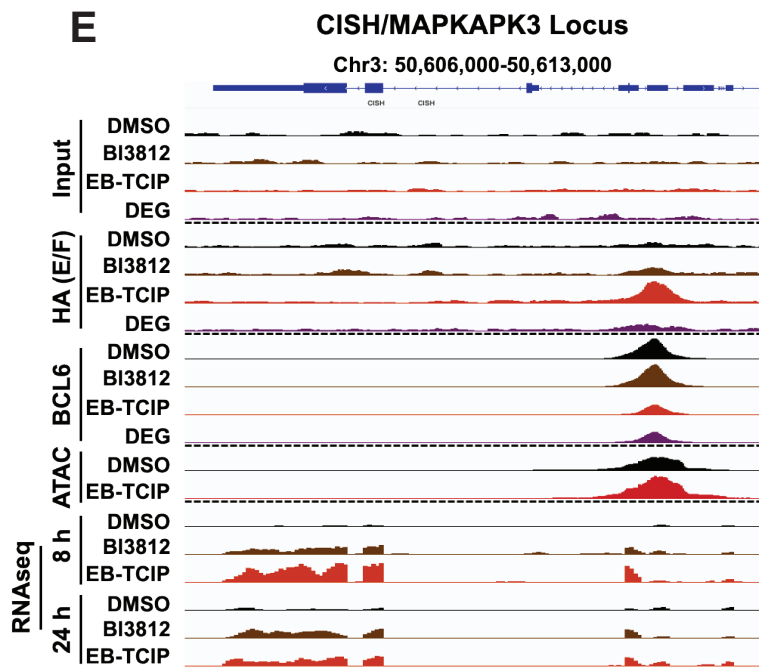
**C**



**D**



**E**



1266 **Figure 5: EB-TCIP changes the localization of FKBP-EWS/FLI1 on chromatin.** (A) ChIP-seq  
1267 tornado plots of HA (FKBP-E/F) binding signal of **EB-TCIP** (red) versus DMSO (black) peaks that  
1268 are decreasing (DEC; 92), non-significantly changing (NS; 8656), and increasing (INC; 2296).  
1269 Differential peaks between **EB-TCIP** and DMSO are shown for all compounds. Compared to **BI3812**  
1270 (brown) and **BI3802 (DEG**, purple), **EB-TCIP** increases FKBP-E/F binding at a subset of genes.  
1271 Line plots for all compound treatments in each cluster are shown to the right. (B) Scatter plot  
1272 portraying top enriched motifs of HA binding sites in DMSO treated cells. (C) Scatter plot portraying  
1273 top motifs of HA increased peaks enriched in **EB-TCIP** treated cells. The BCL6 motif scores 29<sup>th</sup>.  
1274 IGV visualization of Input, HA (FKBP-E/F), BCL6, ATAC-seq signal, and RNA-seq signal at the  
1275 *SOCS2* (D) and *CISH* (E) with treatments DMSO (black), 1  $\mu$ M **BI3812** (brown), 1  $\mu$ M **BI3802 (DEG**,  
1276 purple), and 1  $\mu$ M **EB-TCIP** (red). All ChIP-seq and ATAC-seq is portrayed as the average of two  
1277 independent replicates. RNAseq is portrayed as the average of three independent replicates.